TNO
Material Solutions
Fontys University
of Applied Sciences

The Effects of carboxylic Acids on $CaCO_3$ homogeneous Scale Formation studied by Dynamic Light Scattering

Jacobs, Bram

Supervisors:

Supervisors TNO:	**Yunqi Wang**
	Frank Vercauteren
Supervisor Fontys University of Applied Sciences:	**Arie Demper**

Eindhoven, August, 2020

The Effects of carboxylic Acids on Homogeneous $CaCO_3$ Scale Formation studied by Dynamic Light Scattering

Bachelor graduation thesis
From 1 December 2019 until 11 July 2020

TNO Material solutions
High Tech Campus 25
5656 AE, Eindhoven
The Netherlands

Fontys University of Applied Sciences
De Rondom 1
5612 AP, Eindhoven
The Netherlands

Student: **Bram Jacobs**
bram.jacobs@student.fontys.nl

Supervisors TNO: **Yunqi Wang**
y.wang@tno.nl
Frank Vercauteren
frank.vercauteren@tno.nl

.....

Supervisor Fontys University of Applied Sciences: **Arie Demper**
a.demper@fontys.nl

Samenvatting

CO_2 emissies in Nederland moeten met 40% gereduceerd worden in 2030 vergeleken met 2015. Een groot deel van deze uitstoot komt uit warmteproductie. Om deze emissiedoelstellingen te halen, moet de verwarmingssector in 2030 een reductie van 20 megaton CO_2 hebben gerealiseerd. Een veelbelovende alternatieve warmtebron in Nederland is geothermische energie die in 2050 kan voorzien in 23% van de totale vraag naar warmte-energie. Om Aardwarmte een haalbare optie te maken is het belangrijk dat de onderhoudskosten laag zijn. Een groot obstakel bij de ontwikkeling van geothermische energie is de vorming van "scale".

Scale is de vorming van slecht oplosbaren anorganische zouten uit mineraal rijk water. Deze zouten slaan neer in pijpleidingen en warmtewisselaars waardoor de energieproductie afneemt. De meest voorkomende scale is calciumcarbonaat ($CaCO_3$) en is uitgebreid bestudeerd. Er is echter weinig bekend over de interactie tussen reactieve organische verbindingen en de vorming van scale. Het doel van dit onderzoek is om het effect van verschillende veel voorkomende carbonzuren op de homogene nucleatie en het neerslaan van calciumcarbonaat te onderzoeken. Deze effecten werden bestudeerd met dynamische lichtverstrooiing (DLS) bij verschillende verzadigingsverhoudingen (SR) en zuurconcentraties.

Om de effecten van de carbonzuren te onderzoeken is een DLS flow loop ontwikkeld om de scale vorming in de tijd te bestuderen. Met behulp van Scanning Electron Microscopy (SEM) werd het effect van de carbonzuren op de kristalmorfologie onderzocht. Om de DLS-experimenten te verbeteren en om het effect van vooraf aanwezige deeltjes op schaalvorming te onderzoeken zijn verschillende experimenten uitgevoerd met toevoeging van silica nanodeeltjes.

Er is geconstateerd dat als gevolg van een grote variatie in deeltjesgrootte van de gevormde $CaCO_3$-deeltjes, de DLS niet in staat is om een representatieve gemiddelde deeltjesgrootte te meten. Desalniettemin steld deze methode ons in staat om belangrijke aspecten van homogene kiemvorming te bestuderen, zoals inductietijd en gevormde relatieve hoeveelheden neerslag door gebruik te maken van de scaled count rate.

Experimentele data toont aan dat azijnzuur, malonzuur, benzoëzuur en citroenzuur allemaal een remmend effect hadden op de vorming van calciumcarbonaatprecipitatie. Zowel de inductietijd als de relatieve hoeveelheid neerslag werden beïnvloed door de carbonzuren.

Door de toevoeging van lage concentratie zuren werd geen significante verandering in de $CaCO_3$ kristalmorfologie waargenomen. Verschillende experimenten met relatief hoge zuurconcentraties toonden de vorming van aragonite kristallen aan, die normaal alleen worden waargenomen bij hoge temperaturen.

DLS- en SEM-resultaten toonden aan dat silica-nanodeeltjes de vorming van $CaCO_3$ -precipitatie verhoogden. Door nanodeeltjes te gebruiken, kan de reactie worden gestuurd om kleinere kristallen te produceren wat voordelen kan hebben en mogelijk ook de deeltjesgrootte-analyse door DLS mogelijk maakt.

Abstract

CO_2 emission in the Netherlands must be reduced by 40% in 2030 compared to 2015. A large contributor to the CO_2 emissions is the heating sector. To meet these emission goals the heating sector needs to achieve a reduction of 20 megatons CO_2 by 2030. A promising alternative heat source in the Netherlands is geothermal energy which can meet 23% of the total heat energy demand in 2050. To make geothermal energy a viable option the operation costs have to be low. One major obstacle in the development of geothermal energy is the formation of scale.

Scale is the formation of inorganic sparingly soluble salts present in subsurface waters. These salts precipitate in pipe lines and heat exchangers, decreasing energy production. The most common scale is calcium carbonate ($CaCO_3$) and has been widely studied. However, little is know about the interaction between reactive organic compounds and the formation of scale. The goal of this research is to investigate the effect of several common Carboxylic acids on the homogeneous nucleation and precipitation of Calcium Carbonate. These effects were measured by Dynamic Light Scattering (DLS) at several saturation ratio's (SR) and acid concentration.

To investigate the effects of the carboxylic acids a DLS flow loop was developed to measure the scale formation over time. With the use of Scanning Electron Microscopy (SEM) the effect on the crystal morphology were investigated. To improve the DLS experiments and to research the effect of particulates on scale formation several experiments were conducted with addition of silica nanoparticles.

It was found that due to a large particle size variation of the formed $CaCO_3$ particles the DLS is not able to measure a representative mean particle size. Nevertheless this method allowed us to study important aspects of homogeneous nucleation like induction time and relative amounts of precipitate formed by using the scaled count rate.

Experimental data shows that Acetic acid, Malonic acid, Benzoic acid and Citric acid all had an inhibiting effect on the formation of Calcium carbonate precipitation. Both induction time and relative amount of precipitate were influenced by the carboxylic acids.

No significant change in $CaCO_3$ crystal morphology was observed due to the addition of low concentrations of the acids. Several relatively high acid concentration experiments showed the formation of aragonite crystals, normally only observed at high temperatures.

DLS and SEM results showed that silica nanoparticles increased the formation of $CaCO_3$ precipitation. By using nanoparticles the reaction can be steered to produce smaller crystals which also might make the particles size analysis by DLS possible.

Preface

This graduation thesis describes the work of my graduation project as a graduate student at the Fontys University of Applied Sciences in Eindhoven. This graduation project is executed at TNO in the Material Solutions research group. This research was conducted within the Geothermal Energy program of TNO and is part of the EU funded REFLECT project. The goal of this research was to investigate the effect of several Carboxylic acids on the precipitation and formation of Calcium Carbonate scale in the liquid. These effects were studied by Dynamic Light Scattering at several saturation ratio's and Acid concentrations. In a separate study parallel to this research heterogeneous deposition of scale on surfaces is studied using MATLAB image processing in which I helped developing and optimizing the MATLAB code.

I would like to thank my TNO supervisors Yunqi Wang, Frank Vercauteren and Francesco Pizzocolo and my Fontys supervisor Arie Demper for guidance during my graduation thesis. I would like to thank Margo Segers and Willie Hardeman for giving me SEM instructions at respectively TNO and Fontys. Finally, I would like to thank all other interns and co-workers at the department for their help and feedback during my research.

Nomenclature

Symbols

REFLECT	Redefining geothermal fluid properties at extreme conditions- to optimise future geothermal energy extraction	
EU	European Union	
SR / SI	Saturation Ratio / Saturation Index	
Me	Ion activity cations	(mol/L)
An	Ion activity anions	(mol/L)
K_{sp}	Solubility product	$((mol/L)^2)$
A_i	Ion activity	
C_i	Concentration of ion	(mol/L)
F_i	Activity coefficient	
z_I	Charge of ion	
I	Ionic strength of the solution	(mol/L)
ΔG_{crit}	Critical free energy change	(KJ/mol)
γ	Interfacial tension	(J/m^2)
R_c	Critical size radius	(m)
J	Rate of nucleation	$(\#/cm^3/s)$
A	Nucleation Rate constant	
ΔG	Free energy	(KJ/mol)
K	Boltzmann constant	$(1.380649 * 10^{-23} J/K)$
T	Temperature	(K)
v	Molecular volume	(M^3/mol)
φ	Critical size factor for heterogeneous nucleation	
θ	Contact angle	$(^\circ)$
R_G	Growth rate of crystals	(mol/s)
K_d	Mass transfer coefficient for diffusion	(cm^2/s)
K_r	Mass transfer coefficient for surface integration	(cm^2/s)
C	Solute bulk concentration	(mol/L)
C_{ci}	Solute concentration at crystal interface	(mol/L)
C_{eq}	Equilibrium concentration	(mol/L)
^{n}	Order of integration process	
$S(t)$	Actual covered area by crystals	$(\%)$
$S_{ext}(t)$	Extended area covered by crystals	$(\%)$
M	Molar mass	(g/mol)
K_1	Lateral growth rate	$(mol/\mu m/s)$
N_o	Number of active nucleation sites	(μm^{-2})
A_n	Nucleation rate	
t	Time	(s)
ρ	Density of crystals	$(g/\mu m^3)$
DOC	Dissolved carbon	(mol/L)
P_{CO_2}	Partial CO_2 pressure	(kPa)
SEM	Scanning Electron Microscope	
EDX	Energy-dispersive X-ray spectroscopy	
DLS	Dynamic Light Scattering	

Chemicals

CO_2	Carbon Dioxide
$CaCO_3$	Calcium carbonate
Mg^{2+}	Magnesium ion
Sr^{2+}	Strontium ion
Ba^{2+}	Barium ion
CO_3^{2-}	Carbonate ion
SO_4^{2-}	Sulfate ion
$EDTA$	Ethylenediaminetetraacetic acid
$NaHCO_3$	Sodium Bicarbonate
$CaCl_2 \cdot 2H_2O$	Calcium Chloride Dihydrate
$NaOH$	Sodium Hydroxide
HCl	Hydrogen Chloride
CH_3COOH	Acetic acid
$CH_2(COOH)_2$	Malonic acid
C_6H_5COOH	Benzoic acid
$C_6H_8O_7$	Citric acid
SiO_2	Silicon Dioxide

Contents

1. Introduction

CO_2 emissions in the Netherlands must be reduced by 40% in 2030 compared to 2015 and by 95% in 2050. 40% of Dutch emissions are due to heat consumption. To meet these goals, the heating sector must achieve a reduction of 20 megatonnes (Mton) CO_2 by 2030. [1] To achieve these CO_2 goals, it is necessary to use all available sustainable technologies (wind, solar, biomass, soil energy and geothermal energy). Geothermal energy can potentially reduce CO_2 emissions by 3 Mton by 2030 and 12 Mton by 2050. As seen in figure 1.1 geothermal energy can meet 5% of the total demand for heat in 2030 and 23% in 2050. For geothermal energy to be a viable solution, the operating cost have to be reduced. One large obstacle that stands in the way of low operating costs is the formation of scale.

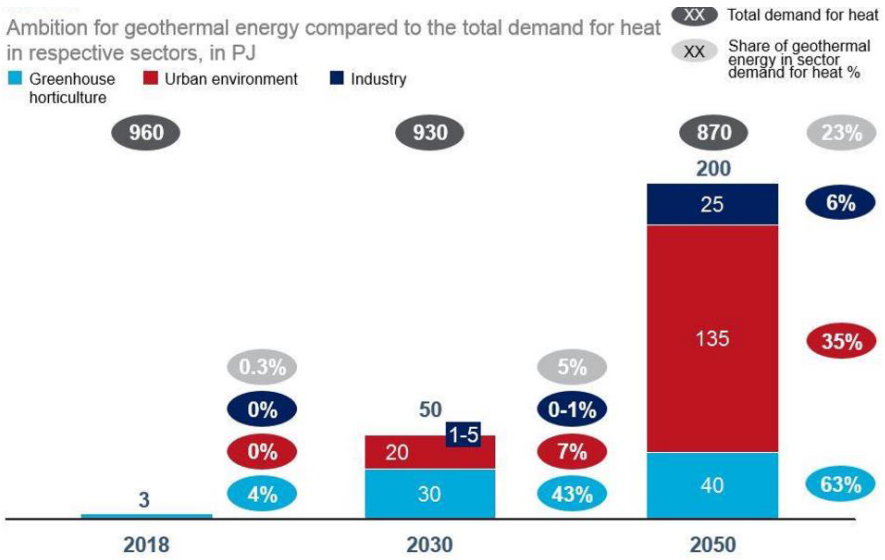

Figure 1.1: Geothermal energy can meet 5% of the total demand for heat in 2030 and 23% in 2050. [1]

Subsurface water contains a number of dissolved species, that can precipitate under certain conditions. The deposition of inorganic sparingly soluble salts from aqueous brines during water, gas or oil production is known as scale. It has a large effect on the flow assurance in a system, and can even reduce the flow to zero. It can cause damage to equipment and lead to a loss in production. Yearly millions of dollars are spent on methods and chemicals to remove or prevent scale formation. Example given the total cost of scale in the oil industry has been estimated to be 1.4 billion dollars. [2]

Redefining geothermal fluid properties at extreme conditions to optimize future geothermal energy extraction (REFLECT) is a EU funded project that aims to prevent problems in fluid chemistry rather then fix them. Properties of liquids in the geothermal cycle are often inadequately defined, REFLECT aims to address this by collecting new, high quality data in critical areas. One of the problems REFLECT focuses on is scale formation. [3]

This study is part of the REFLECT project and focuses on the effect of reactive organic compounds on the formation of Calcium carbonate ($CaCO_3$) scale. The goal is to get a better prediction of scaling in practice by investigating both bulk precipitation and surface deposition under several changing conditions. By using MATLAB in combination with the in-situ scale deposition set up developed by Smetsers [4] deposition of scale on a substrate was studied. In this research Dynamic Light Scattering (DLS) is used to get a better understanding of the effect of reactive organic compounds on the formation of scale in the bulk of the aqueous phase.

Chapter 2 shows the process of scale formation, including a description of supersaturation and nucleation/growth kinetics. The morphology of Calcium carbonate crystals in the precipitate and several scale prevention/removal methods are discussed. Interactions between organic and inorganic compounds in scale formation currently understood are elaborated. Lastly, the researched carboxylic acids are discussed.

Chapter 3 describes the experimental methods and experimental designs that were used in this research. The Dynamic Light Scattering set-up, the Brine compositions and the Morphology analysis using SEM are described. Lastly, the seeded growth and homogeneous vs heterogeneous experiments are discussed.

Chapter 4 presents the effects of concentrations of carboxylic acids on the Calcium carbonate precipitation for Saturation Ratios 5, 9, 15 and 50. The effect on Calcium carbonate crystal morphology is presented using SEM and EDX analysis. Lastly, the results of the seeded growth and heterogeneous experiments are presented. These results are discussed and compared to results presented in literature.

Chapter 5 gives the conclusions over the findings in this research and in chapter 6 recommendations for future research are presented. Lastly, in chapter **??** a reflection of the work done in this research is presented.

Parallel to this research another study is being conducted researching scale formation using MATLAB image processing and the scale-deposition flow rig. In this research I helped developing and optimizing the MATLAB code by creating a GUI and adding new features as can be seen in Appendix C.

2. Theory

2.1 Inorganic Scale Formation

Inorganic scale can precipitate if a situation of supersaturation occurs.The cause of supersaturation can be temperature and pressure changes, mixing of different solutions and chemical reactions. The process of inorganic scale formation can be divided into five stages: initiation, transport, attachment, removal and aging. [5]

2.1.1 Initiation

In the initiation period the surface is conditioned and in the bulk before precipitation, the solution is in a meta stable state where nucleation is impossible. The solution needs to reach an unstable state for nucleation to occur. The time between the beginning of the supersaturation and the onset of precipitation is called the induction time. The induction time for heterogeneous nucleation is influenced by both surface variables (surface temperature, material, surface finish, roughness, and coating) and solution variables (mineral concentration, flow rate, temperature, etc.). For homogeneous nucleation in bulk only the solution variables are of importance. The induction time can vary from several weeks to minutes or seconds. It also offers much potential for the prevention of scale formation. [5, 6]

2.1.2 Transport

In this stage, nuclei formed in the bulk will be transported to a surface. This process depends on the the physical properties of the system and the concentration difference between the surface fluid and the bulk. Diffusion, sedimentation and thermophoresis are a few of the processes that are responsible for the transport. [5]

2.1.3 Attachment

In the attachment stage the nuclei adhere to the surface and among themselves. The salt ions approaching a surface will be attracted due to electrostatic forces and adhere to the surface to grow and and form scale. Material properties such as density, size of the precipitation and surface conditions at the substrate have a big influence on the attachment stage. [5]

2.1.4 Removal

During the scaling process there is competition between the deposition and the removal of the scale. Shear forces at the interface between the scale and the fluid are responsible for the scale removal. The mechanisms that cause the removal are dissolution, erosion and spalling. Spalling describes the process in where fragments are ejected from a body due to impact or stress. [5]

2.1.5 Aging

With the start of the deposition of the scale, the aging process starts. During aging, the crystal may transform to improve or decrease the deposition strength. This means that the mechanical properties of the scale can change due to changes in the chemical or crystal structure. [5]

2.2 Supersaturation

Supersaturation is the driving force behind the formation of scale. Supersaturation arises when the concentration of a mineral in solution is higher than the maximum solubility of this mineral and so a solid phase is formed to get the solution back to an equilibrium. Salts can be grouped into two groups distinguished by their change in solubility at different temperatures: salts whose solubility increases with temperature (normal solubility salts) and salts whose solubility decreases with temperature (inverse solubility salts). [5]

Supersaturation can have different origins:

- Change in temperature
- Change in pressure
- Evaporation of the solution
- Mixing of the solution by adding a substance
- Mixing of two solutions of different composition
- Gas/liquid equilibrium, for example $CO_2(gas) \leftrightarrow CO_2(liquid)$
- Chemical reactions

The saturation ratio, SR, which is an indication of the tendency of the crystallisation to occur, is defined by the following formula:

$$SR = \frac{Me * An}{K_{sp}} \tag{2.1}$$

Where Me is the ion activity of $Mg^{2+}, Ca^{2+}, Sr^{2+}$ or Ba^{2+}, An is the ion activity of CO_3^{2-} or SO_4^{2-} and K_{sp} is the solubility product. The formation of scale can occur when the saturation ratio is larger than 1. The ion activity A_i is defined as the product of the concentration C_i and the activity coefficient f_i and can be seen below. [7, 4, 8, 2]

$$A_i = f_i * C_i \tag{2.2}$$

The activity coefficient for low concentration is given by:

$$log(f_i) = \frac{-0.51 * Z_i^2 * \sqrt{I}}{1 + \sqrt{I}} \tag{2.3}$$

Where Z_i is the ions charge and I is the ionic strength of the solution which is given by:

$$I = \frac{1}{2} * \sum C_i * Z_i^2 \tag{2.4}$$

The Saturation Index SI is related to the Saturation Ratio and can be expressed by the log of SR:

$$SI = log\frac{Me * An}{K_{sp}} \tag{2.5}$$

When SI=0 the solution is in equilibrium with the scale, when SI<0 the solution is undersaturated.

2.3 Nucleation/Growth Kinetics

Crystallization of a system consists of two stages: Nucleation and growth. Nucleation can be split into two types: Primary and secondary nucleation.[9] Primary nucleation occurs in the absence of crystalline material of its own kind. Secondary nucleation is the formation of new crystals in the presence of parent crystals of the same substance. Primary nucleation dominates in scale formation. Primary nucleation can take place either homogeneously or heterogeneously. [4, 8]:

- Homogeneously: Formation of the nuclei without the presence of any solid. (figure 2.1)
- Heterogeneously: Formation of the nuclei in the presence of a foreign solid, for example the surface of the pipeline. (figure 2.1)

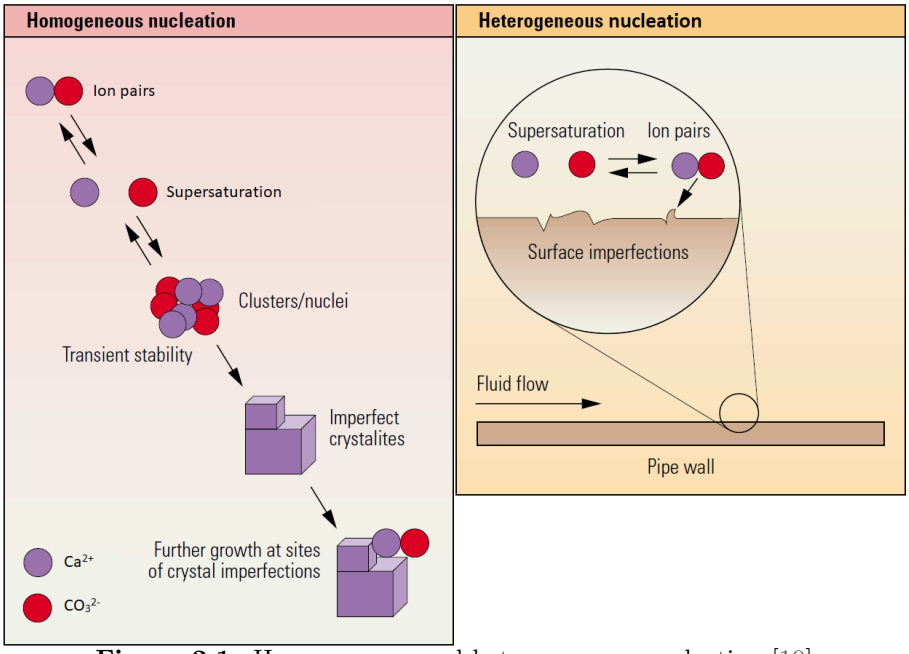

Figure 2.1: Homogeneous and heterogeneous nucleation [10]

If a nuclei is in an environment of high saturation and has a size greater then the critical size it will grow, else it will re-dissolve in the solution. The critical radius is the minimum size that the nuclei is stable. For homogeneous nucleation it can be calculated by determining the critical overall free energy change ΔG_{crit} as represented by the following equation:

$$\Delta G_{crit} = \frac{4\pi\gamma r_c^2}{3} = \frac{16\pi\gamma^3}{3(\Delta G_v)^2} = \frac{16\pi\gamma^3 v^2}{3(KTlnSR)^2} \tag{2.6}$$

Where r_c is the critical size radius, γ is the interfacial tension between the nuclei and the supersaturated solution, ΔG_v is the volume excess free energy, v the molecular volume and SR the saturation ratio, K is the Boltzmann constant and T is the temperature.
The rate of homogeneous nucleation, J, which is the number of nuclei that appear in 1 cm^3 per second, can be expressed in the form of the Arrhenius equation [5, 8, 11]:

$$J = A * exp(-\frac{\Delta G}{KT}) \tag{2.7}$$

Where J is the rate of nucleation, A is a nucleation rate constant, ΔG is the free energy, K is the Boltzmann constant and T is the temperature. This formula can be combined with formula 2.6 as the following:

$$J = A * exp(-\frac{16\pi\gamma^3 v^2}{3K^3T^3 2ln(SR)}) \tag{2.8}$$

It is easier for heterogeneous nucleation to occur than homogeneous nucleation as it requires less free energy change. The overall critical free energy change for heterogeneous nucleation ($\Delta G'_{crit}$) is less than for homogeneous nucleation (ΔG_{crit}) according to [8]:

$$\Delta G'_{crit} = \varphi \Delta G_{crit} \tag{2.9}$$

Where the factor $\varphi < 1$. As heterogeneous nucleation occurs in the presence of a foreign solid and the nucleation rate is a function of the interfacial tension, the interfacial tension between the nuclei, the foreign solid surface and the solution is related by the contact angle θ. With this information the factor φ can be expressed by the following:

$$\varphi = \frac{(2 + cos\theta)(1 - cos\theta)^2}{4} \tag{2.10}$$

Where θ is the angle of wetting for both liquid and solid systems.

2.3.1 Crystal growth

Stable nuclei will grow when found in a supersaturated solution. Many growth mechanisms have been proposed, the two most accepted theories are the diffusion process and the surface reaction process. [8, 12]

- Diffusion process: process in which molecules transport from the solution to the crystal surface by diffusion, convection or both.
- Surface reaction process: process in which molecules incorporate into the surface of the crystal lattice, this is also called surface integration process.

The growth rates for crystal growth for both processes respectively are given by:

$$R_G = k_d(C - C_{ci}) \tag{2.11}$$

$$R_G = k_r(C_{ci} - C_{eq})^n \tag{2.12}$$

Where R_G is the growth rate, k_d and k_r are the mass transfer coefficient for diffusion and surface integration respectively, C is the solute bulk concentration, C_{ci} is the solute concentration at the crystal solution interface, C_{eq} is the equilibrium saturation concentration and n is the order of the integration process.

2.3.2 Progressive and Instantaneous Nucleation

The model by Beaunier et al. [13] and further modified by Euvrard et al. [11] can be used to determine if the nucleation is either instantaneous or progressive. This model assumes that there is a finite number of nucleation sites. When nucleation is instantaneous the nuclei all form in the initial stages of crystal formation and then grow. This means that the nucleation and growth processes are separated and that no further nucleation occurs. Progressive nucleation on the other hand, describes the process where new nuclei will be formed during the whole crystallization process and the number of nuclei will increase over time. (Figure 2.2)

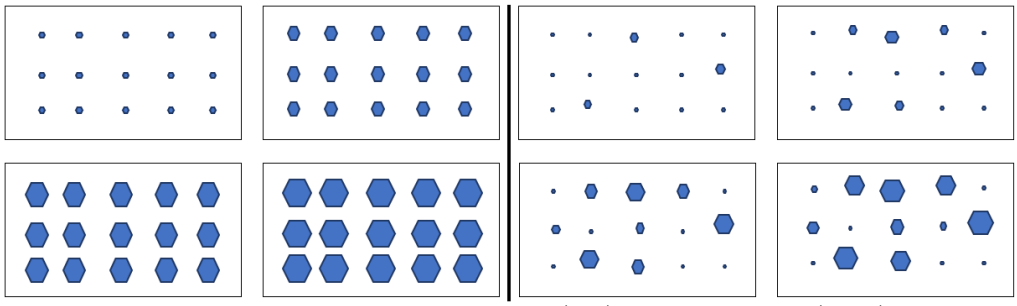

Figure 2.2: Schematic rendering of instantaneous (left) and progressive (right) nucleation. [4]

If we consider growing crystals on a surface, they will eventually overlap, which has an influence on the measurements of number of crystals and the surface of the growing crystals. To solve this problem, Avrami [14] found that the actual covered area, S(t), is related to the area which would be covered without effects of overlap, also called the 'extended area', $S_{ext}(t)$, which is shown in the following formulas [6]:

$$S(t) = 1 - exp(S_{ext}(t)) \tag{2.13}$$

For instantaneous nucleation:

$$S_{ext}(t) = -ln(1 - S(t)) = \frac{MK_1N_0t}{\rho} \tag{2.14}$$

For progressive nucleation:

$$S_{ext}(t) = -ln(1 - S(t)) = \frac{MK_1N_0A_nt^2}{\rho} \tag{2.15}$$

Where M is the molar mass, K_1 is the lateral growth rate, N_0 is the number of active nucleation sites, A_n is the nucleation rate, t is time and ρ is the density of the crystals. Instantaneous nucleation occurs when S_{ext}(t) is proportional to time and progressive nucleation occurs when S_{ext}(t) is proportional to the time squared. [6]
The influence of the Saturation ratio on the nucleation mechanism has been researched by Smetsers [4] and Sanni [6]. It is found that the nucleation mechanism is progressive at low supersaturation ratios and instantaneous at high saturation ratios.

2.4 Scale Prevention and Removal

The industry uses two methods to deal with the formation of scale, scale inhibition and scale removal. Scale inhibition uses chemical treatment to control, reduce or delay scale from forming. Whereas with the use of scale removal methods, the scale is removed after it has already formed in the equipment.

2.4.1 Inhibition

Scale inhibition has been applied very successful over the years to prevent formation of scale in oilfields. It can reduce the rate of scale formation to almost zero. Scale inhibition can be split up into two different methods: (i) nucleation inhibition where the nuclei form but are then disrupted or redissolved by the inhibitor molecules and (ii) crystal growth inhibition where the inhibitor adsorbs or interacts with the crystal active growth sites and stops or slows the growth process. [15, 16]
All inhibitors use both of the above mentioned mechanisms but one mechanism always dominates. It has been established that polymers that are used as scale inhibitors mainly operate as nucleation inhibitors and phosphonates mainly work as crystal growth inhibitors. [15, 17]

2.4.2 Scale Removal

The two most used methods for removing scale are by chemical or mechanical methods. Mechanical removal should only be considered as the last option as it has several limitations. It is very expensive, it requires external drilling equipment and the method will not remove all scale in the system. Thus, chemical methods are preferred for the removal of scale. [16]
Chemical scale removal is often the lowest cost approach and is especially suitable when the scale is not easily accessible. Acidizing is the most widely used method in the geothermal and oil industry. Different carbonate scales, like $CaCO_3$, are soluble in both organic and inorganic acid solutions.

An alternative chemical method is the use of chelating agents such as Ethylenediaminetetraacetic acid (EDTA). Chelating agents have the ability to bind metals such as calcium. Through this process the calcium ions from the scale are bound by the chelating agent. [16]

2.5 Morphology Calcium Carbonate

Calcium carbonate has three crystalline forms: Calcite, Vaterite, Aragonite. These forms have different densities, stabilities and morphological/crystallographic characteristics as can be seen in table 2.1. [6, 4, 8]

Table 2.1: Morphology Calcium Carbonate

	Calcite	**Vaterite**	**Aragonite**
Stability	Most stable	Least stable (Metastable)	More stable (Metastable)
Density	2.711	2.66	2.83
Morphology	Cubic to Rhombohedral	Hexagonal Hemispherical	Needle-like
Crystal Structure	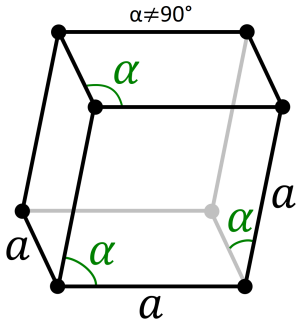	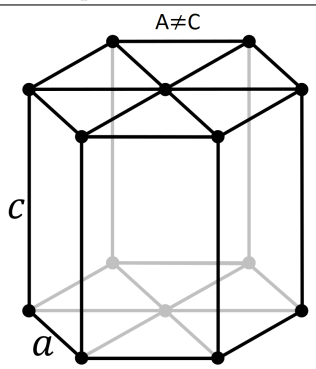	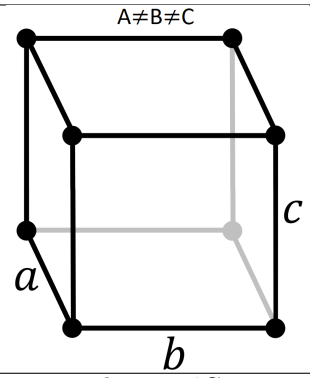
Favoured by	Instantaneous-nucleation Room Temperature High oxygen-Concentration	High supersaturation Low oxygen-concentration Note: Strong tendency-to spread laterally	Temp. above 50°C High pH value (>13.5)
SEM	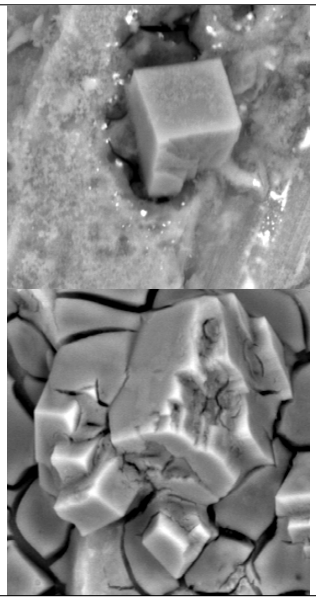	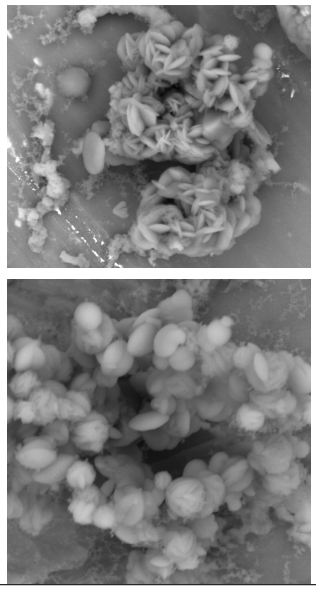	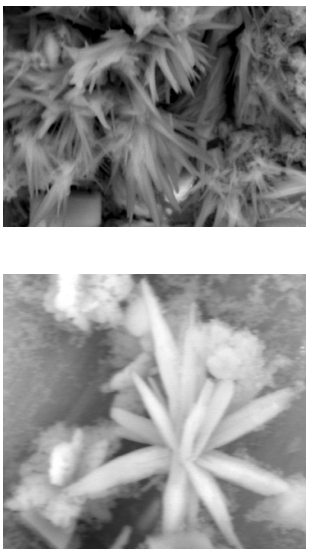

2.6 Interaction Between Organic and Inorganic Compounds

2.6.1 Reactive Organic Compounds in Subsurface Water

Many types of dissolved reactive organic species can be found in subsurface water. They can be split up into three groups: Monocarboxylic acids, Dicarboxylic acids and other reactive organic species. Carboxylic and phenolic groups are most abundant as they are released from the solid organic matter in sedimentary rocks (kerogen) before liquid hydrocarbons are formed. [18, 19]

Monocarboxylic Acids

Monocarboxylic acid anions are the most common organic species in subsurface water. Acetate, propionate, butyrate and valerate are the dominant species within this group. Their concentration is controlled primarily by the temperature and the age of the rocks. Figure 2.3 shows three distinct zones. Zone 1 has a low concentration of Carboxylic acids because of bacteria breaking down the shortchained carboxylic acids. The thermal destruction of bacteria takes place between 60°C and 80°C. This is the reason that in zone 2 the concentration of carboxylic acids is at the maximum. As the temperature gets higher the thermal destruction of the carboxylic acids takes place. This is the reason for the drop in concentration and the very low concentrations in zone 3. Extrapolating this trend gives ∼220°C as the temperature above wich no measurable carboxylic acids are present. [18, 19]

Dicarboxylic Acids

Just as for monocarboxylic acids, the dicarboxylic acid concentration follows the same trend as seen in figure 2.3. However, dicarboxylic acid anions are less stable which means they are found in lower concentrations than monocarboxylic acids. The most common dicarboxylic acid anions found in subsurface water are malonate, succinate and glutarate. [18, 19]

Other Organic Species

Data for concentrations of other reactive organic species are limited. Several amino acids (*e.g., serine, blycine, alamine*) and phenolic compounds (*e.g., phenol, methylphenol, ethylphenol*) have been identified in subsurface waters. Generally, these compounds are found in low concentrations compared to carboxylic compounds. [19]

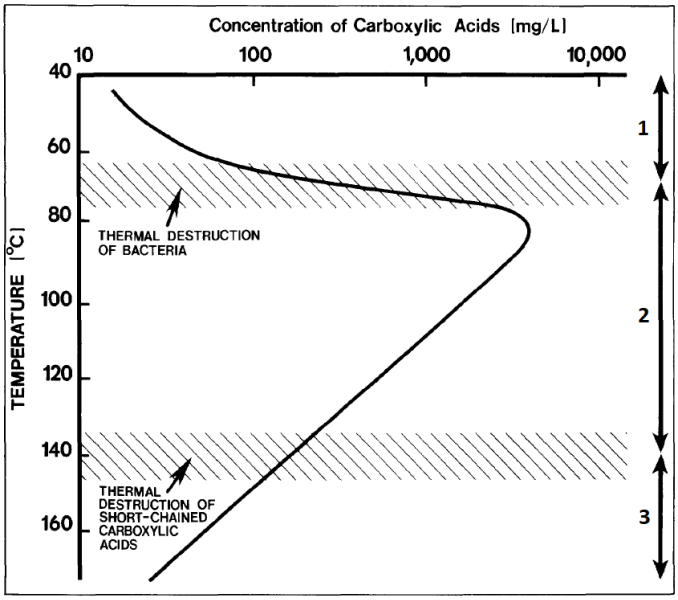

Figure 2.3: Temperature vs Carboxylic Acid concentration, three zones can be identified. [18]

2.6.2 Possible Effects of Organic Compounds on Scale Formation

Several effects of different reactive organic compounds have been researched. Liu et al. [20] found that the absorption of large organic compounds containing a high density of carboxylate functional groups increased $CaCO_3$ crystal size and decreased nucleation time. It is suggested that a high density carboxylate functional groups may enhance surface crystallization by attracting the calcium ions.

Surdam et al. [18] proposes the possibility of the carboxylic acid anions forming salts with calcium ions. These salts have solubility's higher than the $CaCO_3$, which will keep calcium in solution and reduce scale formation.

Lebron et al. [21, 22] researched the effect of organic ligands and the partial CO_2 pressure (P_{CO_2}) on calcite scale formation. It was found that the calcite precipitation rate at certain SR and at P_{CO_2} of 5 and 10 kPa decreased when the dissolved organic carbon (DOC) concentration increased. The DOC concentration needed to be increased to cause an equal reaction at higher P_{CO_2}. It was proposed to evaluate the quantification of the reduction of calcite precipitation due to DOC at different P_{CO_2}.

Kitano et al. [23] researched the effect of organic compounds on the morphology of $CaCO_3$ crystallisation. It was found that the compounds *citrate, malate, pyruvate, glycylglycine and glycogen* greatly reduce the total $CaCO_3$ precipitation and favor the formation of calcite above the other morphology's. Other tested compounds where found to have a moderate effect on the rate of precipitation and mixed effects on the resulting morphology. *Glutamate* caused vaterite and calcite to precipitate; *lactate, chondroitinsulfate, succinate and arginine* favored calcite formation; *glycine and serine* favored vaterite and aragonite precipitation; and *taurine* caused aragonite to precipitate. *Galactose, dextrose, alanine and acetate* where found to have little effect on the precipitation rate and morphology.

Wada et al. [24] found that carboxylic acids interact with the crystal surface of $CaCO_3$. The carboxylic acids distort the crystals morphology by adsorbing to the surface. It was also found that carboxylic acids adsorbed on aragonite nuclei at the start of the crystallization process and inhibited their growth. Wada et al. [25] also found that carboxylic acids are effective growth modifiers, but have no influence on the nucleation of $CaCO_3$. This phenomenon can be explained by the fact that carboxylic acids have a stronger affinity for $CaCO_3$ than for free Ca^{2+} ions.

2.6.3 Carboxylic acids used in experiments

The organic compounds chosen to research are all carboxylic acids as these are the most common organic species in subsurface water and have been researched before. [18, 23, 25]
The Carboxylic acids chosen are Acetic Acid (CH_3COOH), Malonic Acid ($CH_2(COOH)_2$), Benzoic Acid (C_6H_5COOH) and Citric Acid ($C_6H_8O_7$). Acetic, Malonic and Citric Acid have respectively one, two and three carboxylic acid groups as can be seen in figure 2.4. Using these acids, the effect of more carboxylic acid groups in the acid molecule can be researched. To research the effect of other groups attached to the carboxylic acid, Benzoic Acid has been chosen as it has a aromatic group attached to the acid group. Table 2.2 shows the maximum acid concentration observed in subsurface water. Concentration chosen in this research are based on these values and are further discussed in chapter 3.1.

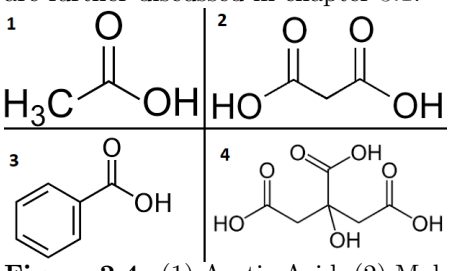

Figure 2.4: (1) Acetic Acid, (2) Malonic Acid, (3) Benzoic Acid, (4) Citric Acid

Table 2.2: Maximum reported acid concentrations in subsurface waters [19]

Carboxylic acid	Maximum reported concentration (mmol/L)
Acetic acid	170
Malonic acid	24
Benzoic acid	0.033
Citric acid	0.021

3. Experimental

3.1 Set-up Bulk Precipitation with Dynamic Light Scattering (DLS)

In figure 3.1 and 3.2 the set-up used for determining the bulk precipitation is shown. In this set-up, both 100ml of $NaHCO_3$ solution and 100 ml of $CaCl_2$ solution are mixed in a beaker at the start of the measurement. The reaction that takes place after mixing is:

$$\mathrm{NaHCO_3 + CaCl_2 \xrightarrow{H_2O} CaCO_3\downarrow + NaCl + HCl.}$$

For the detection of the $CaCO_3$ particles, a DLS-set-up based on the 3D cross correlation geometry as developed by LS Instruments was used. (LS Instruments Nanolab 3D) The Nanolab 3D consists of a laser which emits light at a wavelength of 685 nm. This light is directed at the dispersion through a polarization maintaining optical fiber. The scattered light by the particles at 90° with respect to the incident beam is collected by a second optical fiber. This specific set-up is based on two simultaneous light scattering experiments performed on the same sample by two beams and two detectors. The signals seen by the detectors are cross-correlated which enables the DLS to measure flowing samples. [26, 27]

An Ismatec pump (Reglo Digital ISM832) pumps the mixed solution through a flow-cuvette in the DLS and back into the beaker creating a loop. By using this flow loop the formation of particles over time can be studied. The solutions are prepared by dissolving (A) moles of $NaHCO_3$ and (B) moles of $CaCl_2$ in 1 or 2 liters of Milli-Q water. The nominal values are shown in table 3.1. Exact compositions can be found in appendix B and deviate a maximum of 5% from the concentrations in table 3.2. Mixing both solutions 1:1 results in a solution with the saturation ratio given in table 3.1. Before use in the experiments all solutions are filtered through a 0,22 µm membrane filter to minimize unwanted particles that can influence the DLS measurement. Between experiments the set-up is cleaned with a HCl solution.

Table 3.1: Brine compositions

Saturation Ratio	$NaHCO_3$ **(mol/L)**	$CaCl_2$ **(mol/L)**
5	0.005	0.005
9	0.0075	0.0075
15	0.01	0.01
50	0.0235	0.0235

*For comparison the $K_{sp} = 4,7E^{-9}$ which corresponds to a concentration of 0,00069 mol/L of $NaHCO_3$ and $CaCl_2$.

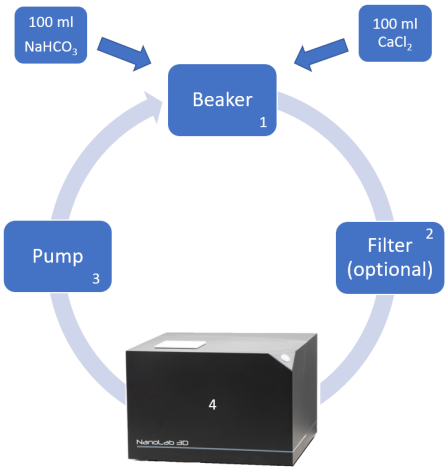

Figure 3.1: Schematic drawing of the DLS set-up.

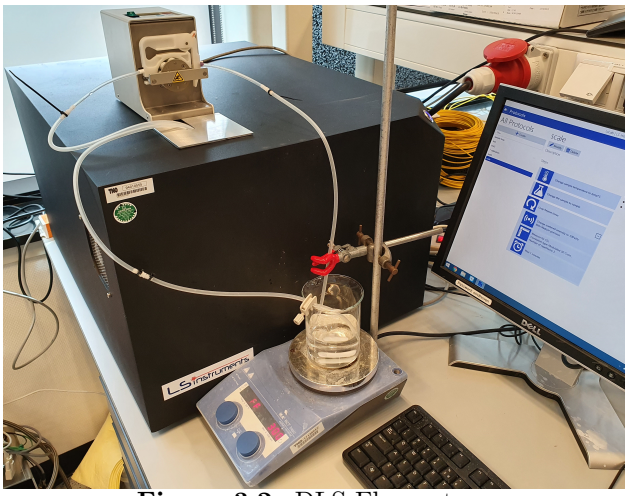

Figure 3.2: DLS Flow set-up

To study the effects of the carboxylic acids mentioned in chapter 2.6.3 on the formation of $CaCO_3$ precipitate various amounts of these acids were added to the $NaHCO_3$ solutions as shown in table 3.2. Exact concentrations can be found in appendix B. After addition of the acids the pH was brought back to the level it was before the addition, approximately 8,7 with a ≈1M $NaOH$ solution. This has been done to avoid the effect of pH on the formation of precipitation and focus on the carboxylic acids. A list of all experiments can be found in Appendix A.

Table 3.2: Carboxylic acid concentrations

Saturation Ratio	**Acetic Acid** (mmol/L)	**Malonic Acid** (mmol/L)	**Benzoic Acid** (mmol/L)	**Citric Acid** (mmol/L)
9	0.9 9.0	0.25 0.5 1.0		
15	0.9 4.5 9.0 18.0 45.0	0.25 0.5 0.75 1.0	0.4 2.0 4.0	0.05 0.1 0.25
50	0.9 4.5 9.0 18.0 45.0 90.0	0.25 0.5 1.0 5.0 10.0	4.0 8.0 12.0 16.0	0.1 0.25 2.5

3.1.1 DLS Programming

The DLS measurements follow a preprogrammed set of steps as seen in figure 3.3. Before the start of the experiment the DLS brings the sample chamber up to a predetermined temperature ranging from 25 to 80 $°C$. When the temperature is reached the software pauses, at this time both solutions are mixed and the pump is started. When the solution reaches the cuvette in the DLS, the software can be unpaused and the measurement starts. The DLS measures two times 15 seconds at a scattered intensity of 100 Khz and then waits for one minute after another measurement is conducted. These steps are repeated until a predetermined amount of measurements is reached.

The main value the DLS produces is the mean particle radius in nm. This value will not be used in this research as the $CaCO_3$ particles grow to fast and too large for a reliable particle size measurement, this will be further discussed in chapter 4.1.

Another value produced by the DLS is the "count rate". This value represent the average scattering intensity during the specific measurement of the specific sample, under the specific optical settings and is measured in khz/mW. Because the DLS uses attenuators to only let a certain amount of light pass to protect the sensor this value can not be linked directly to the particle concentration. To fix this the DLS produces a value called "scaled count rate" in which the attenuator factor is used to produce a theoretical count rate at 100% light intensity. This scaled count rate is in relation with the particle concentration of the sample. A higher scaled count rate indicates a higher concentration and or larger particles. [28] This means that an increase in total precipitation over time can be seen as an increase in count rate over time. If the count rate decreases after reaching a maximum, sedimentation is occurring somewhere in the system. The sedimentation results in less particles in the solution which in turn results in a lower observed count rate. By determining the onset of the increase in scaled count rate the induction time can be determined. This onset is the start of the precipitation and therefor indicates the end of the induction time.

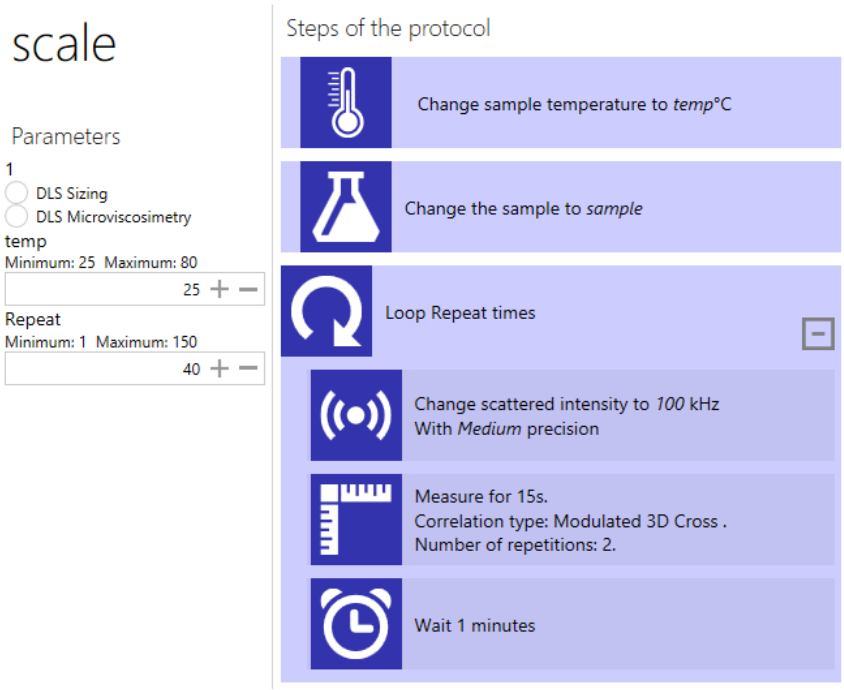

Figure 3.3: Screenshot of DLS software used in experiments.

3.2 Seeded growth experiments

To improve the DLS experiments and to research the effect of particulates that are present in the solution beforehand, several experiments have been conducted using silica nanoparticles (SiO_2). These particles have been added to the $NaHCO_3$ solution before the start of the experiment. The nanoparticles used in these experiments was Levasil CC301, a colloidal silica suspension with 28,1% solids by weight and a nominal particle size of 7 nm. These experiments have been conducted at SR5 to minimize homogeneous nucleation. The pH at the start of the experiments is set at ≈9,5 due too the fact that at this low supersaturation no precipitation occurs at pH 8,7 as used in the before mentioned experiments.

3.3 Homogeneous vs heterogeneous experiments

To research if there is a difference in induction time between homogeneous and heterogeneous nucleation in the DLS experiments several steel sample plates have been introduced in the beaker (Figure 3.1). These sample plates are cut from the same steel substrate that was used by Smetsers. [4] Before mixing the SR15 $CaCl_2$ and the SR15 $NaHCO_3$ solutions the five 2x2 cm plates were halfway submerged into the liquid and fixed in place. The first plate was removed when precipitation started as observed by the DLS. Subsequent plates were taken out every five minutes. All plates were analysed with a DINO-lite AM4515T5 microscope in combination with a MATLAB procedure to analyse the number and size of the particles deposited.

3.4 Morphology

To research the effect of the carboxylic acids on the morphology of the calcium carbonate crystals, samples have been taken at the end of each experiment for Scanning Electron Microscopy (SEM). These samples have been centrifuged at 1200rpm for 15 minutes to concentrate the particles. The liquid layer has been removed and the particles have been washed with Milli-Q water to reduce the high concentrations of still dissolved salts in the solution. After this wash step the samples have been centrifuged again at 1200 rpm for 15 minutes. No dissolution of scale particles was observed. A portion of the particles have been removed with a pipette and deposited on a sample holder. These samples were dried overnight at room temperature after which SEM and Energy-dispersive X-ray spectroscopy (EDX) measurements were conducted. EDX measurements result in a energy spectrum where each peak corresponds with a chemical element. This way the elemental composition of the specimen can be measured Both the SEM at Fontys (Phenom World) and the SEM at TNO (FEI Quanta 600) were used for analysis.

4. Results and Discussion

This chapter shows and discusses the obtained results from various experiments using the DLS-flow set-up. The influence of the carboxylic acids on the precipitation and the morphology are presented for SR50, SR15 and SR9. This data is followed by experiments looking at the influence of the presence of silica nanoparticles at SR5 and experiments comparing homogeneous and heterogeneous nucleation.

4.1 Basis of comparison experiments

To research the effect of the four carboxylic acids on the $CaCO_3$ precipitation a basis of comparison had to be established. To generate this basis several precipitation experiments have been conducted where no acids were added into the mixture at saturation ratios of 50, 15, 9 and 5.

4.1.1 Precipitation

In figure 4.1 the scaled count rates of the above mentioned experiments are shown over time. The end time of the experiment are an estimate that is made beforehand. This estimation is the reason the total measurement time differs between experiments. At SR50, SR15 and SR9 an increase in count rate over time is observed, indicating the formation of $CaCO_3$ participate. At SR5 no precipitation occurred during the 4 hours the experiment ran and so no increase in count rate is observed. As the saturation ratio decreases an increase in induction time, indicated by the onset of the increase in scaled count rate, is observed until no precipitation occurs anymore during the experiment. The maximum scaled count rate decreases as the saturation ratio decreases, indicating that less precipitation is formed as the saturation ratio decreases. This is in agreement with Sanni and Smetsers [6, 4]

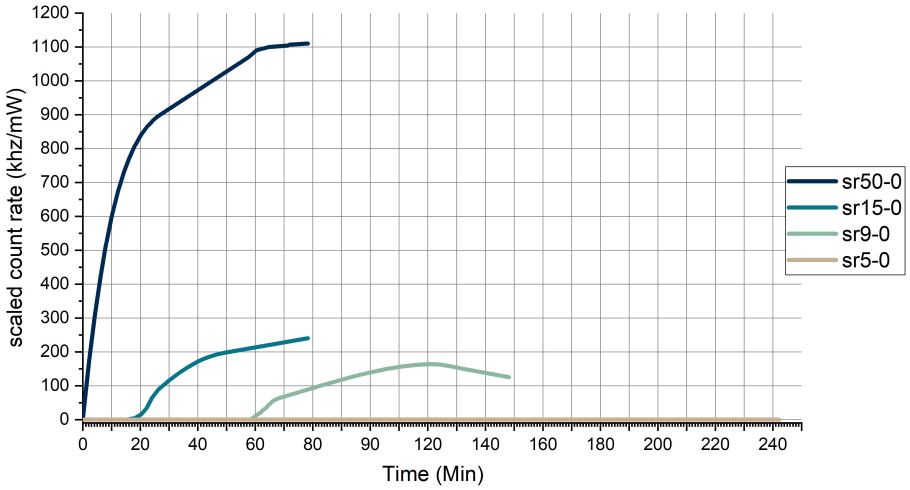

Figure 4.1: Scaled count rate of $CaCO_3$ precipitation at SR50, SR15, SR9, SR5.

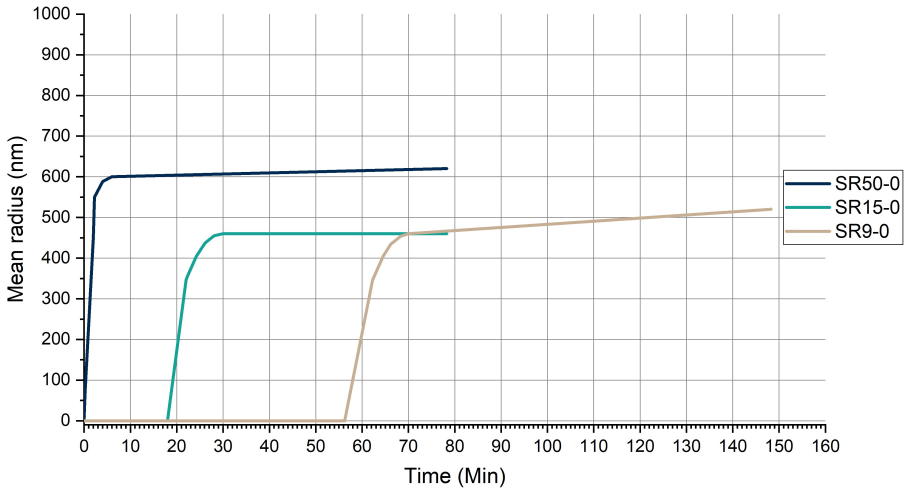

Figure 4.2: Mean Particle Radius of $CaCO_3$ precipitation at SR50, SR15, SR9, SR5.

In figure 4.2 the Mean particle radius over time of the $CaCO_3$ crystals at SR50, SR15 and SR9 is shown. At all three saturation ratios a steep increase in particle radius is observed at the start of precipitation after which the radius stabilizes at around 500 nm. To verify the measured particle radius SEM samples were taken and are shown in 4.4 and 4.5. In these SEM images a large variation in particle size is observed. These particles range from below 100 nm to above 10 µm. Due too this large variation in particles size the radius measured by the DLS is influenced. A few large particles can overshadow many smaller particles. Another problem is that the particle size limit of the DLS is 10 µm, any larger particles will distort the measurement and will give results that are not representative. As this large variation in particle size is observed in most experiments conducted in this research the Particle radius measured by the DLS is not used for further analysis. Nevertheless this method allows us to study important aspect of homogeneous nucleation like induction time and relative amounts of precipitate formed by using the scaled count rate.

4.1.2 Reproducibility

To research the reproducibility of the experiments several identical experiments with no addition of acid have been conducted at SR50 and SR15 and can be seen in figure 4.3 and appendix D. These experiments show no measurable variance in induction time at SR50 as it is very short. The results of SR15 on the other hand show an induction time that ranges from 6 to 18 minutes indicating that other factors in the set-up have an influence on the precipitation.

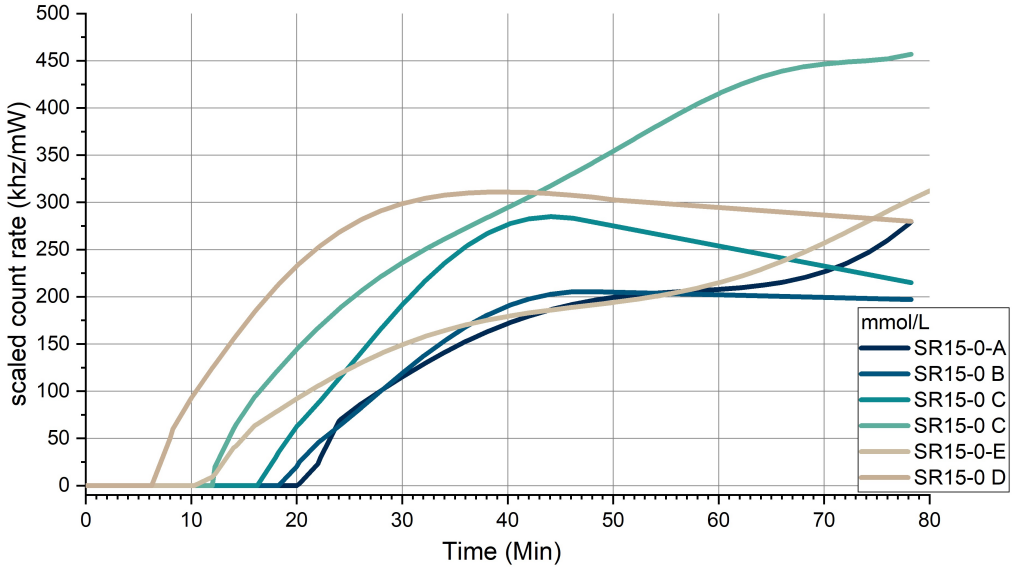

Figure 4.3: Scaled count rate of $CaCO_3$ precipitation at SR15, six identical experiments were conducted with no addition of any acid.

One of the factors might be the storage time of the used $NaHCO_3$ and $CaCl_2$ solutions. The composition and pH of these solutions might change a little over time by reacting with the surrounding air resulting in changes in the Saturation Ratio. Another factor might be that the set-up is an open system, particulate's in the air might settle in the beaker and resulting in heterogeneous precipitation to occur.
Due too this 12 minute variation in induction time at low saturation ratio's, it can be concluded that changes in induction time, that fall within this variation, might not be caused by the addition of the carboxylic-acids and are a result of the set-up used.

4.1.3 Morphology

To find a basis of comparison for the $CaCO_3$ morphology, samples have been taken at the end of the experiments. These samples have been analysed with SEM and SEM-EDX. As well as the large variation in particle size, several morphologies of $CaCO_3$ can be observed in the SEM images. The two most abundant morphologies are Cubic crystals and spherical/hexagonal crystals which correspond to calcite and vaterite respectively.

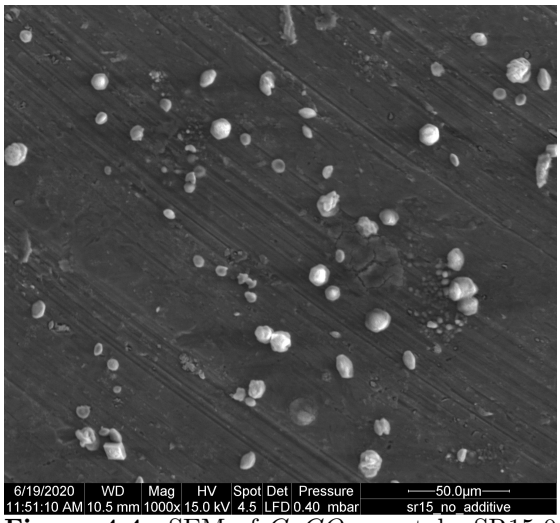

Figure 4.4: SEM of $CaCO_3$ crystals, SR15-0 (1000x)

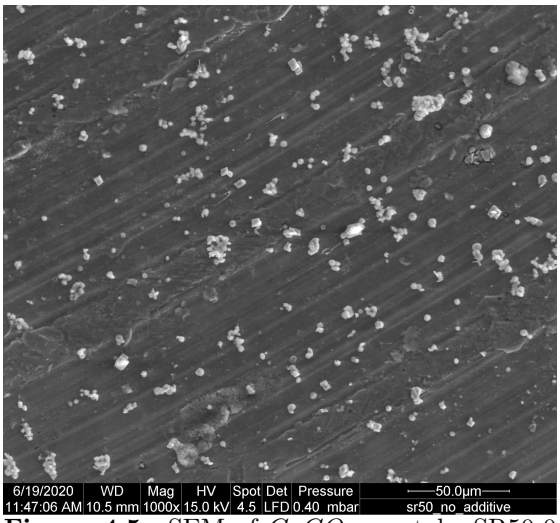

Figure 4.5: SEM of $CaCO_3$ crystals, SR50-0 (1000x)

EDX measurements of both samples confirm that these particles are $CaCO_3$ as can be seen in figure 4.6 by the peaks that correspond with oxygen, carbon and calcium. The aluminium peak is a result of the composition of the sample holder. Lastly a small peak that corresponds with sodium is observed. This is a result of drying the sample during the preparation of the SEM samples which solidifies the still dissolved salts. The SEM-EDX images have less detail due to the fact that these have to be taken at high vacuum while all other SEM images are taken at low vacuum to reduce the charging of the samples. Further differences in morphology will be discussed in chapter 4.6

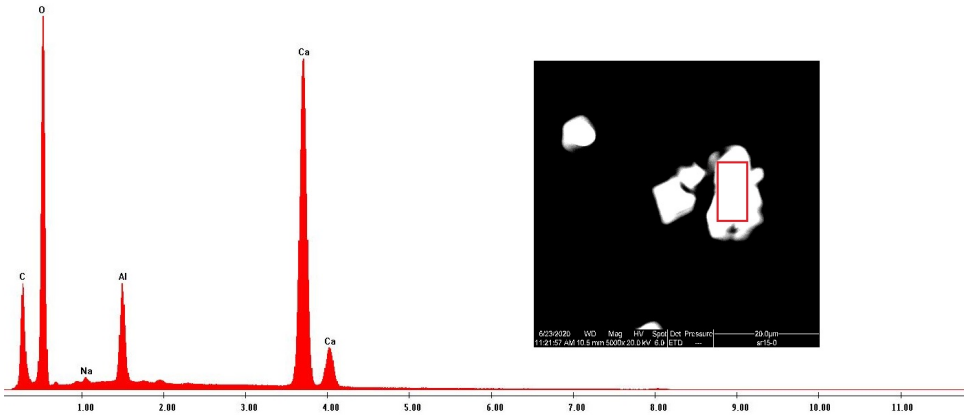

Figure 4.6: EDX measurement of SR15-0 sample, analysed area is the area in the red square.

4.2 Influence of carboxylic acids at SR50

To determine the influence of acetic acid, malonic acid, benzoic acid and citric acid at SR50 several experiments have been conducted in which increasing concentrations of acid have been added to the mixture of $NaHCO_3$ and $CaCl_2$. These experiments are compared with the results in chapter 4.1 and are discussed below.

In figure 4.7 the effect of acetic acid at SR50 is shown. In all experiments the precipitation starts instantaneously and no effect on the induction time is observed as shown by the onset of the count rate. As the concentration of acetic acid is increased, a decrease in total precipitation is observed as seen by the decrease in maximum count rate. At a acetic acid concentration of 18 mmol/L this drop was first clearly observed. At a concentration of 0,9 and 4,5 mmol/L acetic acid a drop in count rate is observed at the end of the experiment. However this drop is caused by sedimentation in the flow cuvette which decreases the measurable particle concentration in the solution which in turn results in a lower count rate. This phenomenon is observed in several other experiments in this research as well.

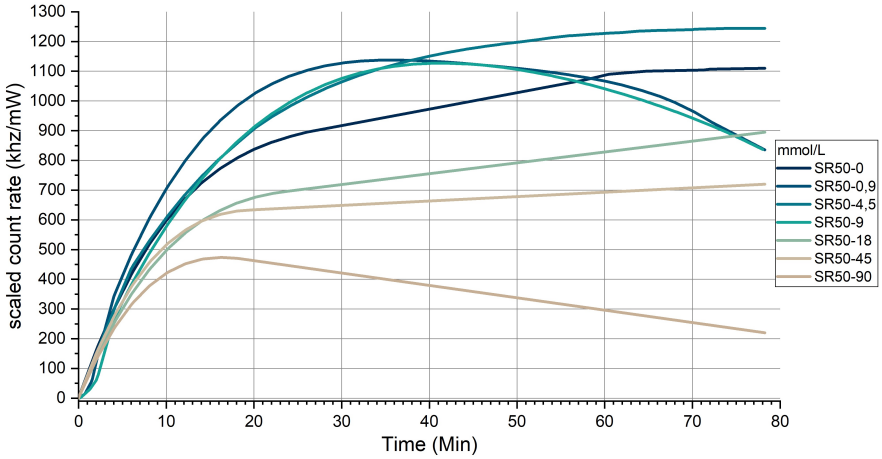

Figure 4.7: Scaled count rate of $CaCO_3$ precipitation at SR50 after addition of Acetic Acid.

In figure 4.8 the effect of malonic acid at SR50 is shown. Again no difference in induction time was observed. A decrease in maximum count rate was observed as the acid concentration increased. At a malonic acid concentration of 0,5 mmol/L this drop was first clearly observed. This decrease starts at a much lower acid concentration in comparison with acetic acid (0,5 mmol vs 18 mmol). Above 0,5 mmol acid concentration sedimentation is also observed in the cuvette and is shown as a drop in scaled count rate in figure 4.8. This may be attributed to the presence of bigger particles in these experiments compared to experiments at 0 and 0,25 mmol/L Malonic acid.

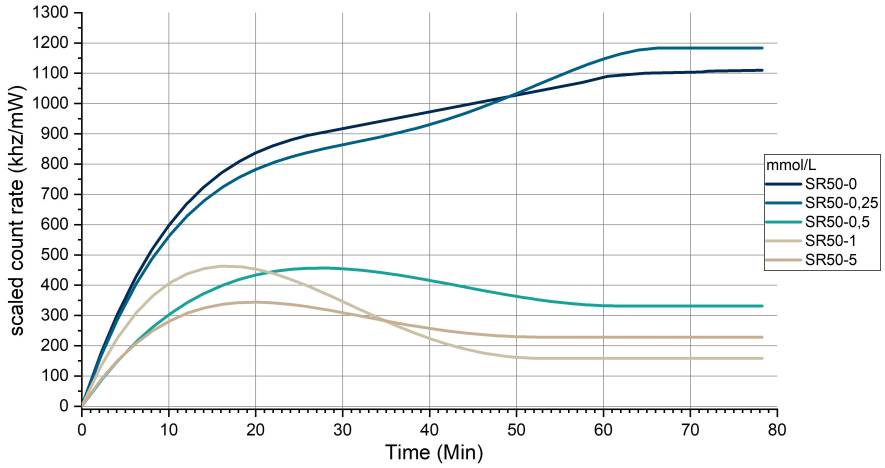

Figure 4.8: Scaled count rate of $CaCO_3$ precipitation at SR50 after addition of Malonic Acid.

The effect of citric acid at SR50 is shown in figure 4.9. For the first time an increase in induction time, indicated by the onset of the count rate, is observed as acid concentration increases. Again a decrease of the maximum count rate is observed with increasing acid concentrations. This decrease is observed at even lower acid concentrations in comparison to acetic and malonic acid (0,1 vs 0,5 mmol/L). At 2,5 mmol/L citric acid concentration no precipitation was observed during the experiment.

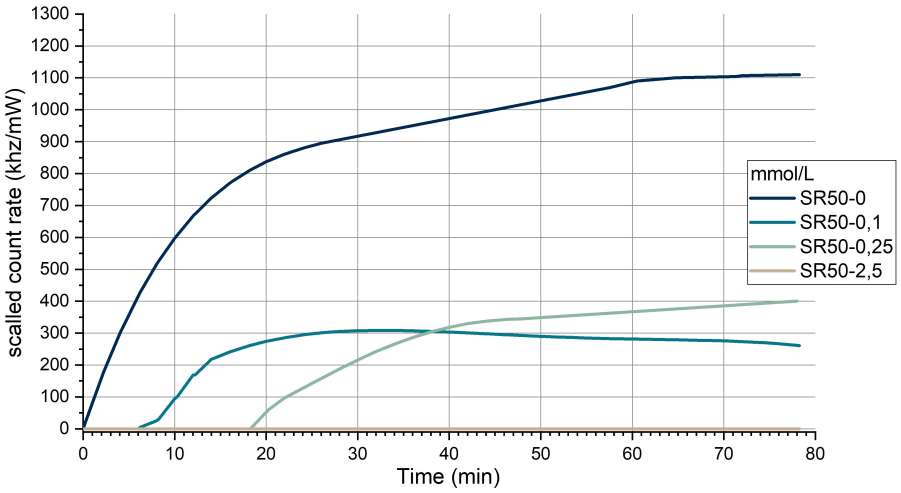

Figure 4.9: Scaled count rate of $CaCO_3$ precipitation at SR50 after addition of Citric Acid.

In figure 4.10 the effect of benzoic acid at SR50 is shown. A decrease in maximum count rate is observed and no increase in induction time is observed as acid concentration increases. At 12 mmol/L benzoic acid concentration and above no precipitation was observed during the experiment. At a concentration of 8 mmol/L benzoic acid sedimentation occurs in the cuvette as indicated by the drop in count rate after reaching a maximum.

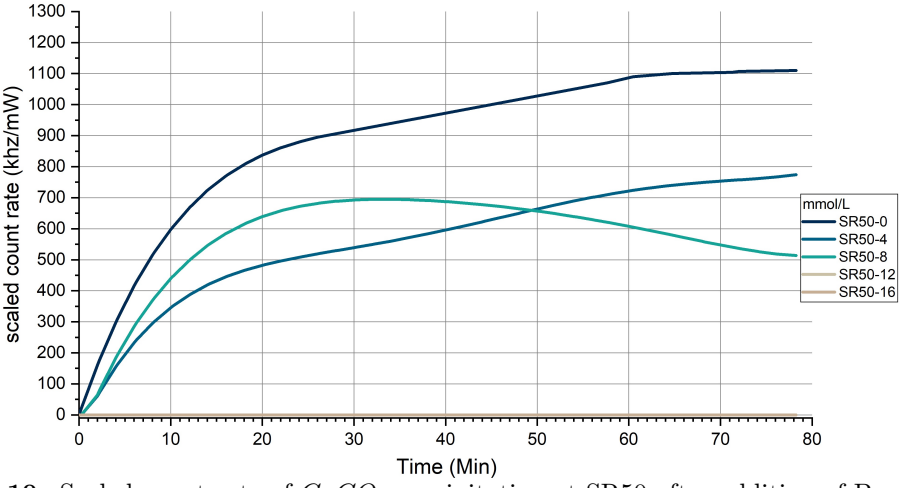

Figure 4.10: Scaled count rate of $CaCO_3$ precipitation at SR50 after addition of Benzoic Acid.

4.3 Influence of carboxylic acids at SR15

To determine the effects of acetic acid, malonic acid, benzoic acid and citric acid at SR15 several experiments have been conducted in which increasing concentrations of acid have been added to the $CaCl_2$ and $NaHCO_3$ mixture. These experiments are compared with the results in chapter 4.1 and are discussed below.

The effect of acetic acid at SR15 is shown in figure 4.11. Already without addition of acid, the count rate is considerably lower than at SR50. In contrast to SR50, an increase in induction time is observed as acid concentration increases. A decrease in maximum count rate is observed as well. The induction time is increased from 16 minutes at 0 mmol/L to more than 130 minutes at 9 mmol/L and above. As induction time increases total precipitation decreases. In comparison to SR50 the onset of the decrease in total precipitation is observed at lower acid concentrations.

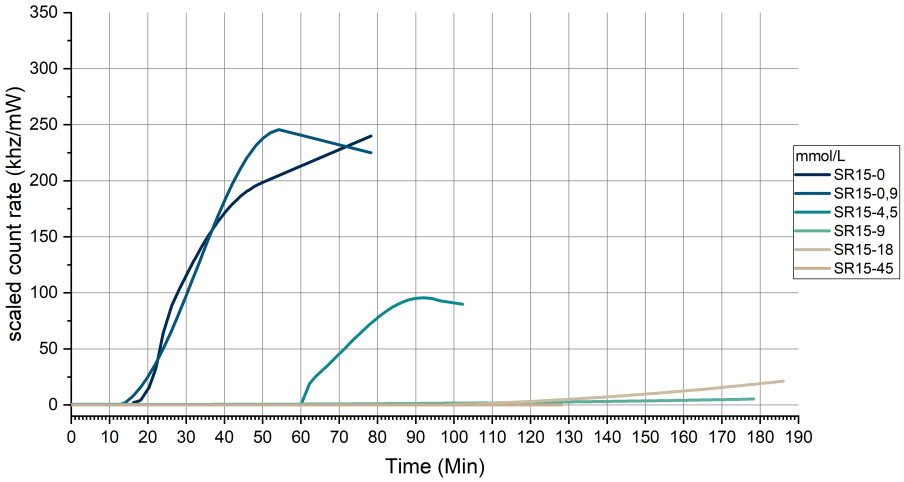

Figure 4.11: Scaled count rate of $CaCO_3$ precipitation at SR15 after addition of Acetic Acid.

Figure 4.12 shows the effect of malonic acid at SR15. An increase in induction time and a decrease in maximum count rate is observed as acid concentration increases. The induction is increased from 16 minutes at 0 mmol/L to more than 50 minutes at 0,75 mmol/L and above. In comparison to SR50 the effect of Malonic acid is larger at lower concentrations.

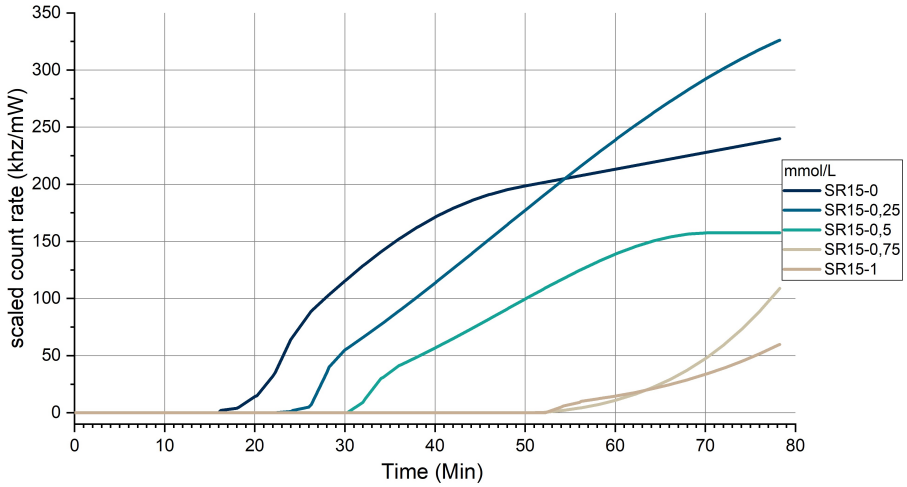

Figure 4.12: Scaled count rate of $CaCO_3$ precipitation at SR15 after addition of Malonic Acid.

In Figure 4.13 the effect of citric acid at SR15 is shown. Both an increase in induction time and a decrease in total precipitation is observed. The induction time is increased from 16 minutes at 0 mmol/L to more then 120 minutes at 0,25 mmol acid concentration. In comparison to SR50 the effect of Citric acid is larger at lower concentrations. In comparison to the acetic and malonic acid the effect is more pronounced and starts at lower acid concentrations.

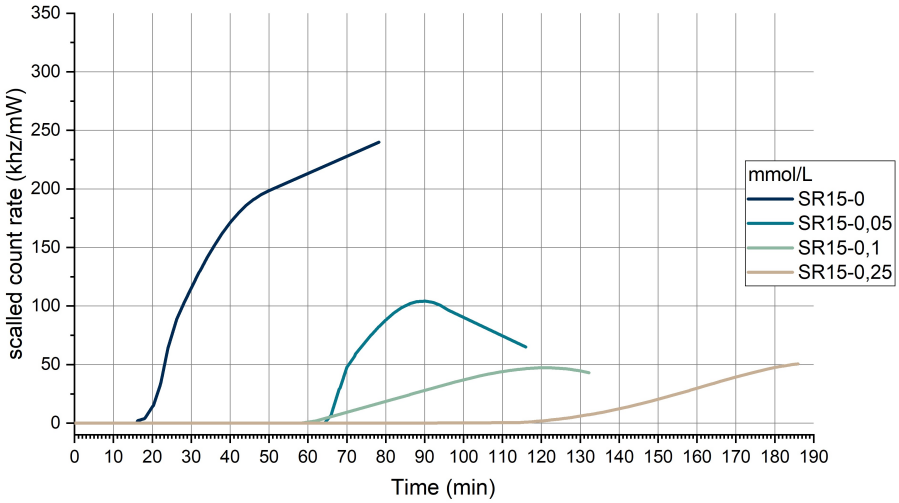

Figure 4.13: Scaled count rate of $CaCO_3$ precipitation at SR15 after addition of Citric Acid.

Figure 4.14 shows the effect of benzoic acid at SR15. In general the same decrease in total precipitation and increase in induction time as the other acids is seen. However, the addition of 0,4 mmol/L benzoic acid seems to show a different trend as more precipitation seems to be formed at first. Several extra experiments have been conducted of this concentration and are shown in appendix D. As discussed in chapter 4.1 the induction time at SR15 varies between 6 and 18 minutes. The measurement of 0,4 mmol/L benzoic acid fits within this variation indicating no significant effect on the $CaCO_3$ precipitation compared to no addition of benzoic acid.

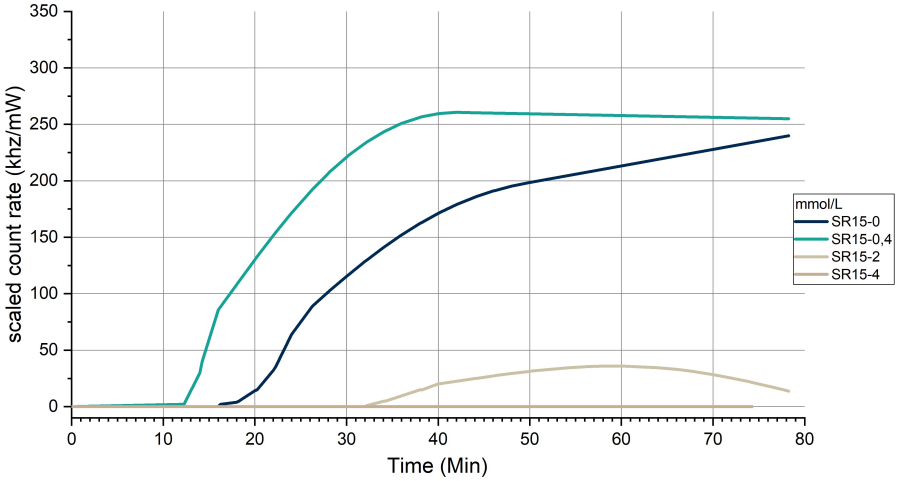

Figure 4.14: Scaled count rate of $CaCO_3$ precipitation at SR15 after addition of Benzoic Acid.

4.4 Influence of carboxylic acids at SR9

To determine the influence of acetic acid, malonic acid at SR9 several experiments have been conducted in which increasing concentrations of acid have been added to the mixture of $NaHCO_3$ and $CaCl_2$. These experiments are compared with the results in chapter 4.1 and are discussed below.

The effect of acetic acid at SR9 is shown in figure 4.15. An increase in induction time and a decrease maximum count rate is observed as acid concentration rises. When compared to SR50 and SR15 these effects are larger at lower acetic acid concentrations. At a concentration of 9 mmol/L acid no precipitation occurs during the experiment. After reaching a maximum, a drop in count rate is observed at a concentration of 0 and 0,9 mmol/L acetic acid. This drop is cause by sedimentation in the cuvette.

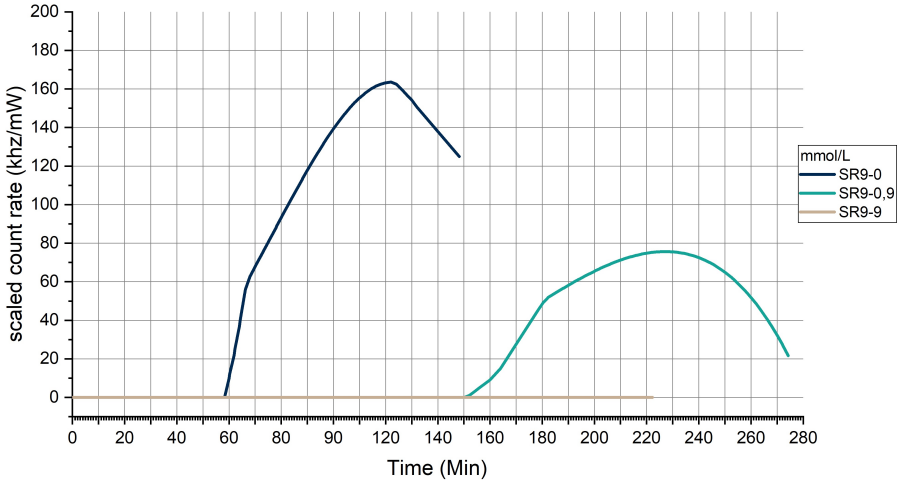

Figure 4.15: Scaled count rate of $CaCO_3$ precipitation at SR9 after addition of Acetic Acid.

Figure 4.16 shows the effect of malonic acid at SR9. Again a decrease in maximum count rate is observed on addition of malonic acid. The induction time does not seem to increase significantly up to a concentration of 0,5 mmol/L. At a concentration of 1 mmol/L malonic acid no precipitation occurs during the experiment. The drop in count rate at 0 mmol/L malonic acid after reaching a maximum is caused by sedimentation in the cuvette as discussed in chapter3.1.1. When comparing these results with SR50 and SR15 the effects on induction time and relative precipitation is larger at lower malonic acid concentrations.

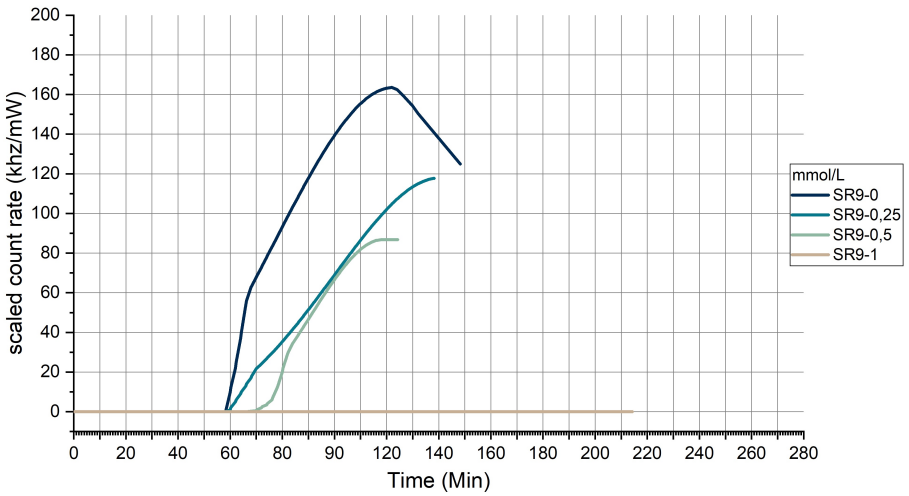

Figure 4.16: Scaled count rate of $CaCO_3$ precipitation at SR9 after addition of Malonic Acid.

4.5 Comparison between carboxylic acids

To further investigate the effects of the carboxylic acids used in this research the DLS results are compared and discussed for the three tested saturation ratios.

4.5.1 SR50

The downward trend in maximum count rate observed after addition of the acids studied, indicates that these acids have an inhibiting effect on the homogeneous nucleation of $CaCO_3$ at SR50. This is in contradiction with Wada et al. [25]. Generally, it is observed that an increase in concentration of acetic acid, malonic acid, benzoic acid and citric acid results in less $CaCO_3$ precipitating. When comparing the acetic, malonic and citric acid results it is shown that less acid concentration is needed to reduce the $CaCO_3$ precipitation as the number of carboxylic acid groups increase. After addition of acetic acid the first significant change in count rate is observed at a concentration of 9 mmol/L (Figure 4.7). In comparison a change in count rate is observed at a concentration of 0,5 mmol/L and 0,1 mmol/L for malonic and citric acid respectively (Figure 4.8 and 4.9). Benzoic acid shows similar results to acetic acid at first until up to a concentration of 8 mmol/L (Figure 4.10). At higher acid concentration benzoic acid stops the precipitation completely within the measured time.
As acid concentration increase, sedimentation in the cuvette is observed more often. This suggest the formation of larger particles. As $CaCO_3$ particle size analysis by the DLS is not possible as discussed in chapter 4.1 and SEM images show no significant increase in particle size, further research is needed to verify this conclusion.

4.5.2 SR15

The inhibiting effect of the acids observed at SR50 is also observed at SR15 but to a higher degree. Both a decrease in maximum count rate and a increase in induction time is observed after addition of acetic acid, malonic acid, benzoic acid and citric acid. Generally, it is observed that an increase in acid concentration results in less $CaCO_3$ precipitating and a longer induction time. When comparing the SR15 results to SR50, lower acid concentrations are needed to have a significant effect on the precipitation. For example malonic acid decreased the precipitation at a concentration of 0,25 mmol/L at SR15 in comparison to 0,5 mmol/L at SR50 (Figure 4.8 and 4.12). This suggests that as saturation ratio decreases the effect of the carboxylic acids increases.

When comparing acetic acid, malonic acid and citric acid it is observed that less acid concentration is needed to reduce the $CaCO_3$ precipitation as the number of carboxylic acid groups increase. This observation is similar to the results of SR50. This confirms that increasing carboxylic groups in a molecule, decreases $CaCO_3$ precipitation and increases induction time. It is also in line with the fact that large molecules with many carboxylic groups are already used as inhibitors for $CaCO_3$ in the industry. [29]

4.5.3 SR9

The downward trend of maximum count rate observed at SR50 and SR15 is also observed at SR9 for Acetic and malonic acid but at an even higher degree. Even lower acid concentrations have an effect on the $CaCO_3$ precipitation compared to SR15. For example acetic acid decreased the precipitation at a concentration of 0,9 mmol/L at SR9 in comparison to 4,5 mmol/L at SR15. (figure 4.11 and 4.15). Again it is observed that malonic acid reduces the $CaCO_3$ precipitation more then acetic acid.

4.6 Influence of carboxylic acids on $CaCO_3$ morphology

A lot of study's have shown that the polymorphism of $CaCO_3$ mainly depends on temperature. [30, 31] To study if the presence of acetic acid, malonic acid, benzoic acid and citric acid has an effect on the morphology of the $CaCO_3$ crystals samples have been taken after the DLS experiments and were analysed by SEM and SEM-EDX.

In table 4.1 the four different morphology's that were observed in the $CaCO_3$ samples are shown. Cubic crystals correspond with calcite, both spherical/hexagonal and flower like crystals correspond with vaterite and needle crystals correspond with aragonite.

Table 4.1: Observed morphology's in $CaCO_3$ samples

Cubic	**Spherical/hexagonal**	**Flower Like**	**Needles**
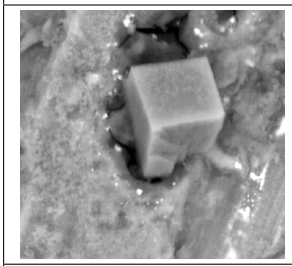	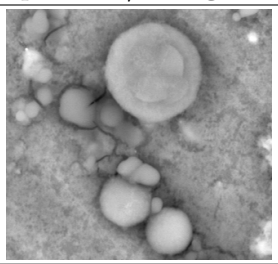	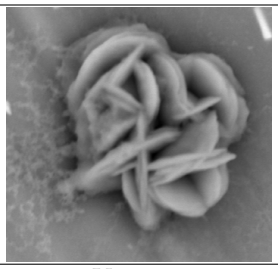	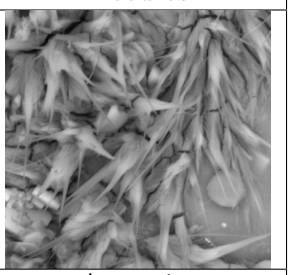
Calcite	Vaterite	Vaterite	Aragonite

In most experiments the carboxylic acids had no observed effect on the morphology of the crystals. Cubic, spherical/hexagonal and flower like crystals were observed in most samples and in a large variation of sizes. The distribution of particles is so chaotic that the distortion of the crystals morphology as reported by Wada et al. [24] can not be observed using this method. Only samples showing new morphology's will be discussed below and are shown in table 4.2. A list of all SEM samples and the observed morphology's is shown in appendix F.

Table 4.2: Sample with changes in morphology

# *	**Sample Name**	**Morphology's**
74	SR9-no additive	Cubic and Needles
68	SR9-0,9mmol/L acetic acid	Cubic, spherical and needles
27	SR15-50°C	Cubic and needles
59	SR50-50°C	Cubic and needles
42	SR50-45mmol/L acetic acid	Cubic, spherical, flower like and needles
43	SR50-5mmol/L malonic acid	Cubic, spherical, flower like and needles

*Full list of experiments can be found in appendix A.

In both samples of 50°C needle crystals were observed corresponding with aragonite and are shown in figure 4.17. This is in agreement with literature [4, 6, 8] as the formation of aragonite is only observed at higher temperatures. Crystal size ranged from 1 µm to more then 10 µm.
Samples of SR9 both with and without the addition of acid showed small crystals that had needle like characteristics and suggested the formation of aragonite which was unexpected. (figure 4.18). EDX of these crystals is shown in figure 4.19. Carbon, oxygen, calcium and chloride peaks are observed. The chloride peak suggests that these particles might not be calcium carbonate. Further analysis with XRD is needed to support this.

Figure 4.17: SEM of $CaCO_3$ crystals, SR50-50°C (5000x)

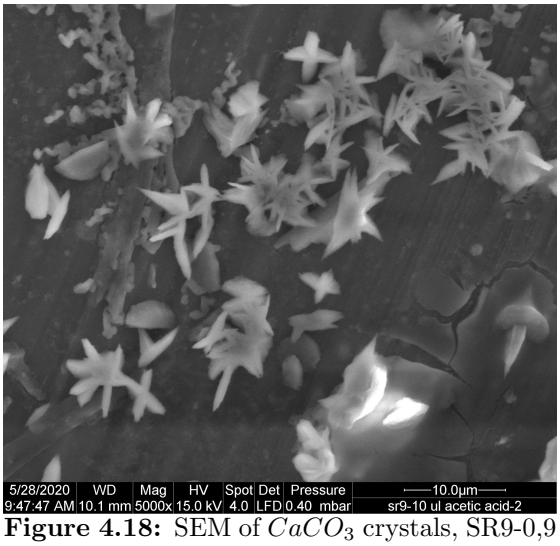

Figure 4.18: SEM of $CaCO_3$ crystals, SR9-0,9 mmol/L acetic acid (5000x)

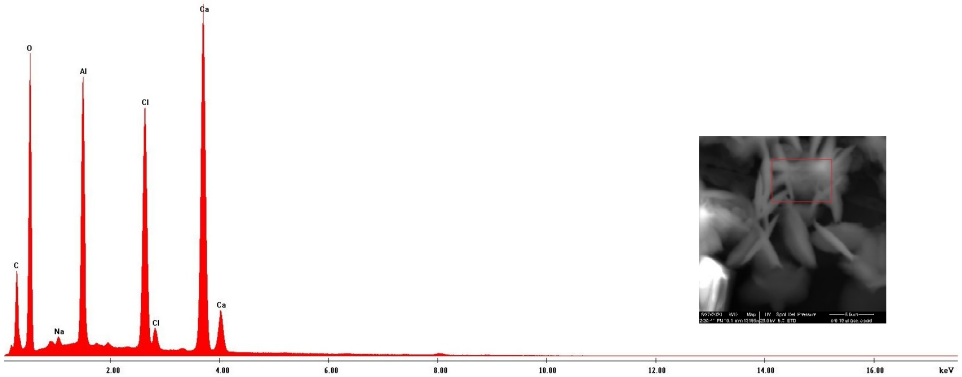

Figure 4.19: EDX measurement of SR9- 0,9mmol/L acetic acid sample

Two samples of SR50, one with 5 mmol/L malonic acid and the other with 45mmol/L acetic acid added showed needle like crystals suggesting the formation of aragonite (Figure 4.20 and 4.21). Both samples have relatively high concentrations of acid added suggesting the possibility that high acid concentrations can change the morphology of $CaCO_3$. Both samples were analysed with EDX and colored maps of the elements present in the samples are shown in figure 4.22 and 4.23.

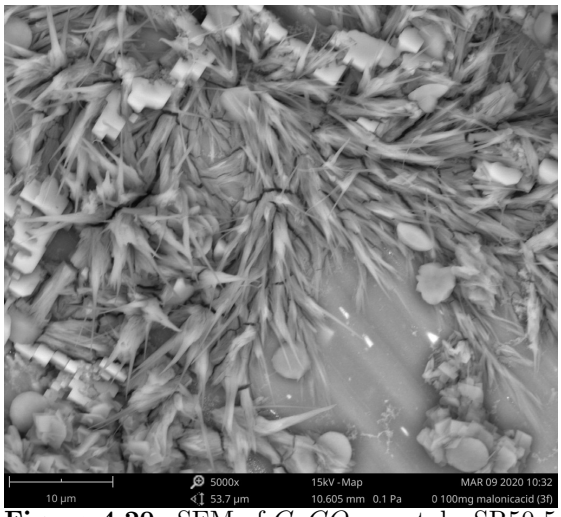

Figure 4.20: SEM of $CaCO_3$ crystals, SR50 5 mmol/L malonic acid (5000x)

Figure 4.21: SEM of $CaCO_3$ crystals, SR50 45 mmol/L acetic acid (5000x)

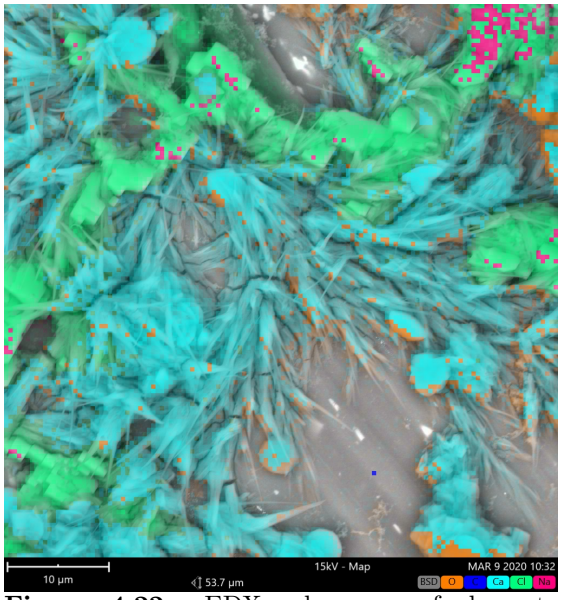

Figure 4.22: EDX color map of elements present SR50 5 mmol/L malonic acid sample

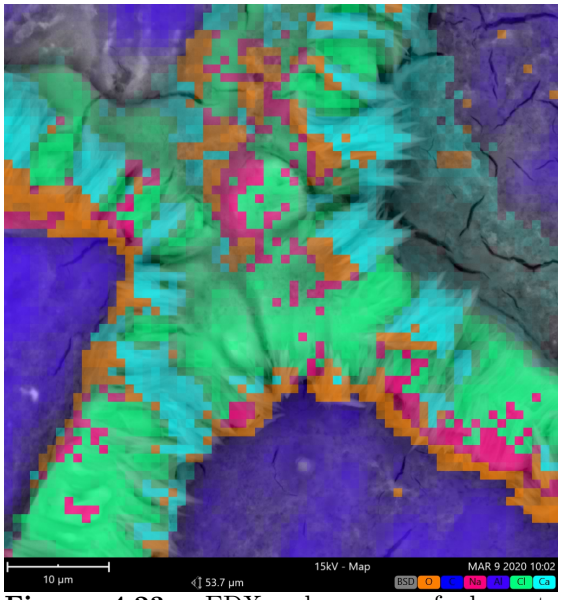

Figure 4.23: EDX color map of elements present SR50 45 mmol/L acetic acid sample

Each color in figure 4.22 and 4.23 correspond to an element most abundant in that location. These maps can give an indication of the elements the observed crystals are made of. The light blue and orange colors in figure 4.22 corresponding to Ca and O respectively, showed that the needle like crystals observed at SR50 with addition of 5 mmol/L malonic acid are most likely aragonite. Contrastingly, the EDX color map of SR50 with addition of 45 mmol/L acetic acid showed several other elements present in the needle like crystals including chloride and sodium. This suggests that these crystals might not be aragonite. The formation of the needles in a cross pattern also suggests the possibility that the needles formed on top of $NaCl$ crystals. This cross pattern is observed elsewhere in the same sample as $NaCl$ and can be seen in figure 4.24. Both these samples need further analysis by XRD to support these observations.

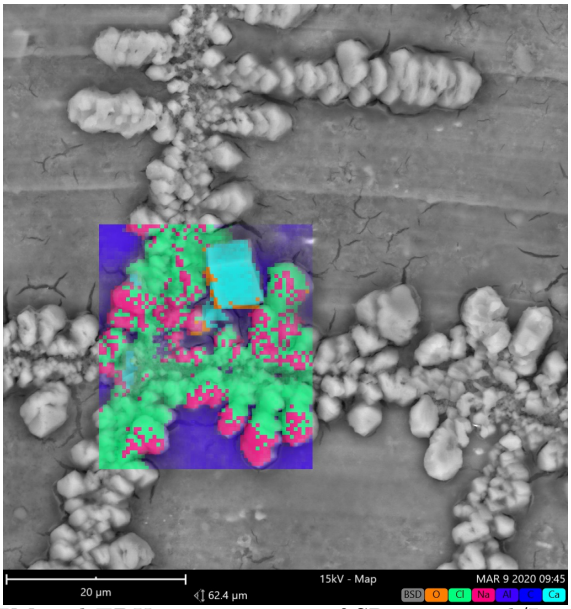

Figure 4.24: SEM and EDX measurement of SR50 45mmol/L acetic acid sample

4.7 Influence of Silica nanoparticles at SR5

To improve the DLS experiments and to research the effect of particulates that are present in the solution beforehand, several experiments have been conducted using silica nanoparticles (SiO_2). Results of these experiments are shown and discussed below.

In figure 4.25 the scaled count rate is shown of three experiments, SR5 at pH of 8.7, SR5 at pH of 9.5 and SR5 at a pH of 9.4 with 0,6 ml Levasil suspension added. At a pH of 8.7 no precipitation is observed for at least 240 minutes. As no precipitation occurs at pH 8.7, the pH has been set to ≈9.5 to initiate precipitation at SR5 within reasonable time as can be seen as the brown line in figure 4.25. The drop in count rate at 20 minutes is due to sedimentation in the cuvette. The subsequent rise in count rate is produced by flushing the cuvette of the sedimentation and mixing the particles back into the solution. The green line in figure 4.25 shows the precipitation in the presence of the SiO_2 seed and shows and increase in maximum count rate in comparison to the experiment without seed. The fluctuation in the count rate is due to sedimentation in the cuvette and subsequently flushing the cuvette. In the presence of the seed particles the effect of sedimentation is smaller. This could indicate that there are less large particles that show sedimentation. To investigate this SEM pictures were taken of the particles that were formed in both experiments at pH 9,5.

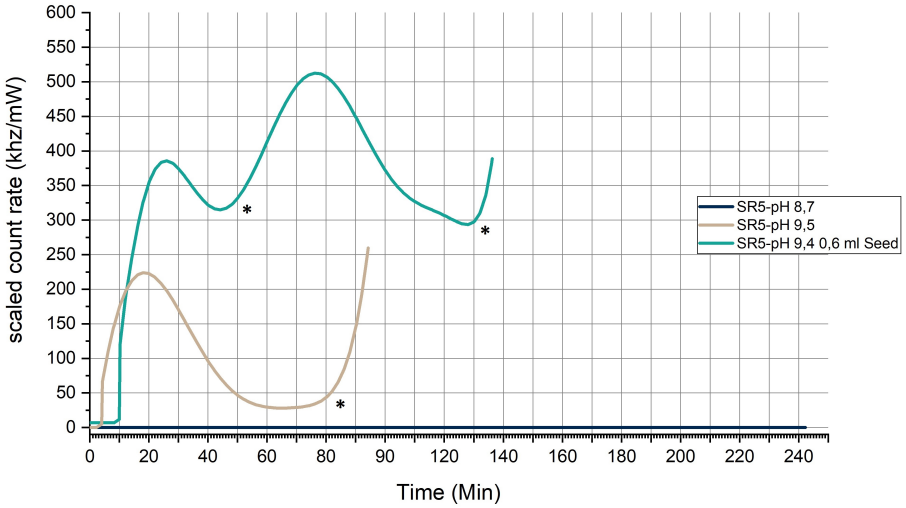

Figure 4.25: Scaled count rate of $CaCO_3$ precipitation at SR5 after addition of Silica nanoparticles.
*Increase in count rate is caused by flushing the cuvette after sedimentation occurred.

The SEM images (Figure 4.26 and 4.27) are in agreement with the DLS results and show more and smaller particles in the seeded sample. Both samples still contain large calcite and vaterite particles but only the seeded sample shows an abundance of small vaterite particles. Analysing these particles with SEM-EDX shows these particle formed around the SiO_2 seeds as can be seen in figure 4.28.

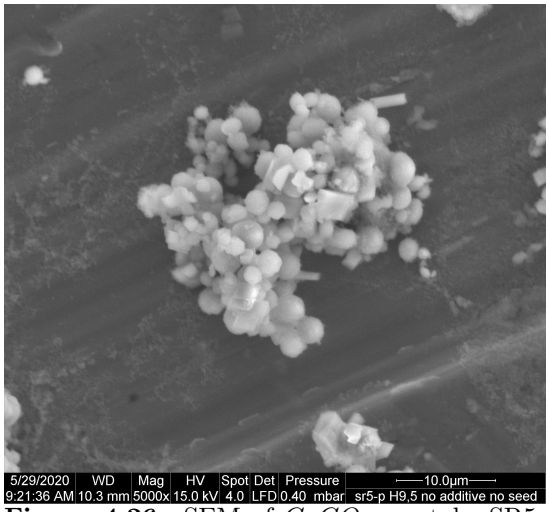

Figure 4.26: SEM of $CaCO_3$ crystals, SR5-pH 9.5 without seeds (5000x)

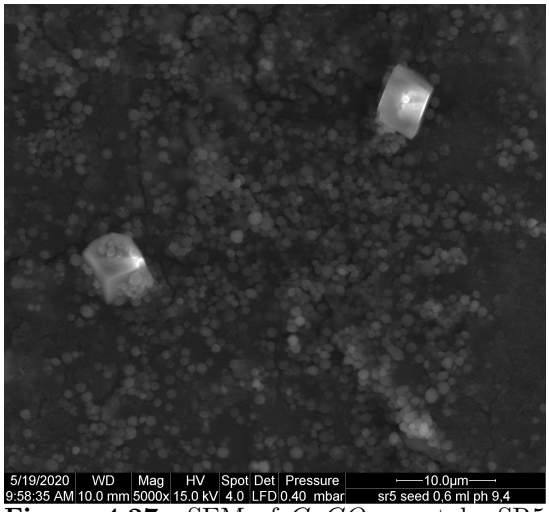

Figure 4.27: SEM of $CaCO_3$ crystals, SR5 pH 9.4 with SiO_2 seeds (5000x)

Silica, calcium, oxygen and carbon peaks are observed in figure 4.28 agreeing with calcium carbonate particles formed around the silica nanoparticles. The aluminium and copper peaks are a result of the composition of the sample holder. This experiment proves that it is possible to steer the particle size of scale by addition of seeds. This might be used as a strategy to avoid the deposition of scale crystals.

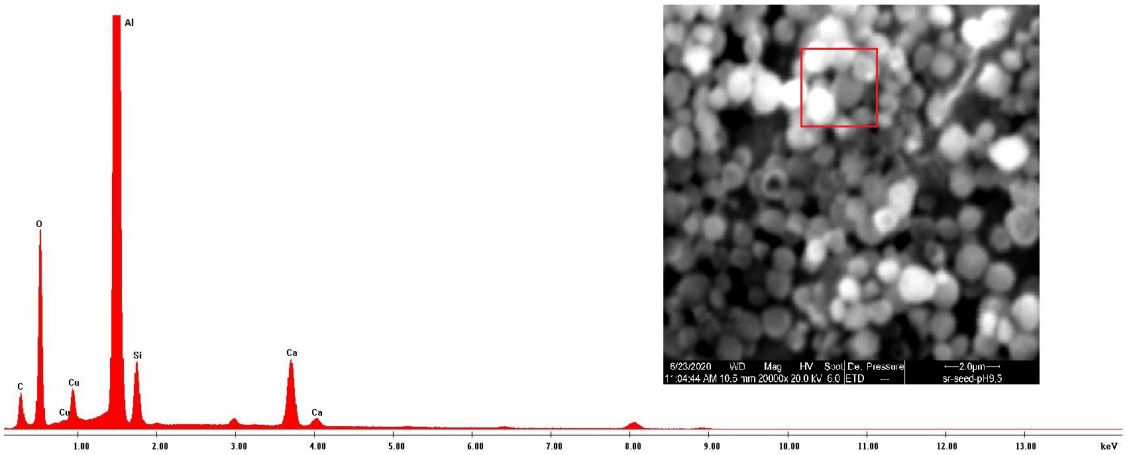

Figure 4.28: EDX measurement of SR5 with SiO_2 seed, analysed area is the area in the red square.

4.8 Homogeneous vs heterogeneous scale formation

To study if there is a difference in induction time between homogeneous and heterogeneous nucleation in the DLS experiments, an experiments has been conducted using the smooth steel substrate used by Smetsers to induce the heterogeneous nucleation.

When the SR15 results of Smetsers[4] are compared to the results in chapter 4.3 it seems that homogeneous nucleation starts before the formation of scale on the surface, as shown by an induction time of 15 vs 70 minutes. This is unexpected as heterogeneous nucleation requires less energy compared to homogeneous nucleation and therefore should occur earlier. To find out if this difference is caused simply by the two different experiment types a comparison experiment of both is performed. Figure 4.29 and 4.30 show an image of the first plate that was taken out during the experiment. This plate was removed at T=20 minutes when the precipitation started. Figure 4.30 shows the with MATLAB processed image of 4.29.
The MATLAB code used is based on block processing to filter out noise and out-of-focus particles. The particles detection is based on the pixel intensity and converts the image into a black and white image. Using this black and white image the particles can be characterized and values such as mean diameter, standard deviations and covered area can be calculated.

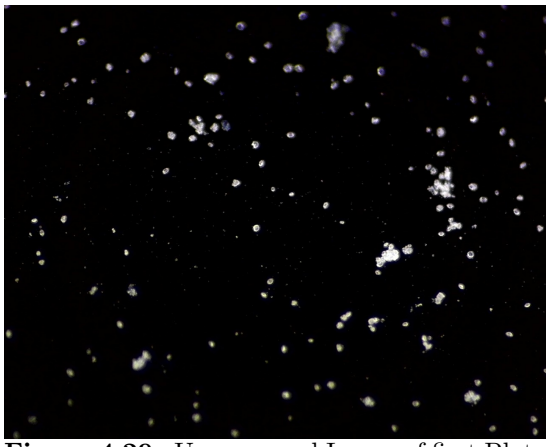

Figure 4.29: Unprocessed Image of first Plate (749x)

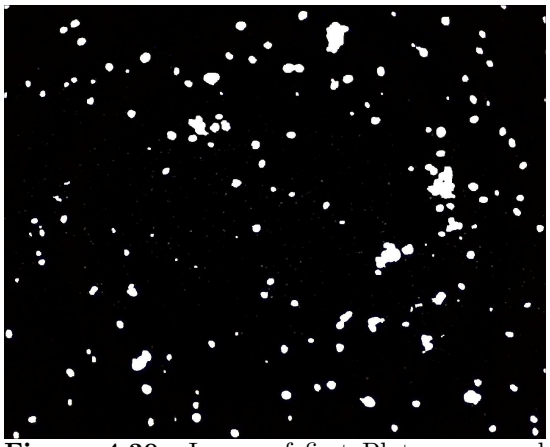

Figure 4.30: Image of first Plate processed with MATLAB (749x)

In these figures scale formation is observed (shown in white) and scale formation was observed on all subsequent plates (Appendix E). This is in contradiction with the results of Smetsers [4] and supports the idea that the difference in induction time is caused by the difference in how the experiments are run. This refers to the fact that the solution in the flow loop is continuously refreshed and the solution in the DLS is recirculated. In the flow loop the solution is mixed 10 cm before the measurement area and is discarded after it passes through the set up. The time it takes for the solution to pass through is maybe too short for particles to form and settle on the substrate at low saturation ratio's. In comparison the solution in the DLS is never refreshed and particles can form in any place in the setup.

5. Conclusion

The goal of this research is to investigate the effect of several common carboxylic acids on the formation of homogeneous calcium carbonate scale. The developed method using dynamic light scattering has proven to be a new method to study important aspects of homogeneous nucleation like induction time and relative amounts of precipitate formed by using the scaled count rate.

SEM results in this study showed broad particle size distribution of the formed $CaCO_3$ particles, which makes it impossible for the DLS to measure a representative mean particle size. However, by using the scaled count rate the effects of acetic acid, malonic acid, benzoic acid and citric acid on homogeneous nucleation of $CaCO_3$ could be studied

All carboxylic acids tested in this research had an inhibiting effect on the precipitation of calcium carbonate. Both the induction time and amount of precipitation was influenced by the carboxylic acids. DLS results show as acid concentration increases induction time is increased and total precipitation is reduced. DLS results also show that as carboxylic groups in the acid molecule increase, less acid concentration is needed to observe the same effect.

In most experiments conducted in this study no significant change in $CaCO_3$ crystal morphology was observed. Several relatively high acid concentration experiments possibly showed the formation of aragonite crystals, normally only observed at high temperatures. Further analysis with XRD is needed to confirm these observations.

DLS and SEM results showed that silica nanoparticles increased the formation of $CaCO_3$ precipitation. SEM-EDX showed that many smaller crystals formed around the silica nanoparticles. By using nanoparticles the reaction can be steered to produce smaller crystals which might make the particles size analysis by DLS possible.

Preliminary experiments showed that the induction time of homogeneous nucleation in this study was shorter then the induction of heterogeneous nucleation researched by Smetsers [4]. This was unexpected as heterogeneous nucleation requires less energy compared to homogeneous nucleation. By analysing both homogeneous and heterogeneous nucleation in the DLS flow loop it was observed that both nucleation types occurred simultaneously and that the initial observation are caused by a difference in experimentation and setup.

6. Recommendations

The DLS flow loop was designed to research the homogeneous formation of scale. It showed that by using the scaled count rate, important aspects like induction time and relative amounts of precipitate can be studied. Further improvement of the flow loop and method is suggested.

One major problem is that the DLS is not able to measure particle size of very poly disperse samples. Several experiments have been conducted in which filters were added in the flow loop to reduce the amount of large particles (Appendix A). These experiments however were not successfull, the filters sucked in extra air creating bubbles in the flow loop and therefore interfered with the DLS measurements. Further research is needed to steer the homogeneous nucleation to create less poly disperse particles. Using particle seeds to initiate the nucleation seems a promising option. Further research in the use of filters is suggested as well.

Researching the effects of organic compounds on other types of scale such as Barium Sulfate and Strontium sulfate is suggested to increase the understanding of scale formation. Experimenting at higher temperatures is also recommended, the DLS setup used in this study is able to measure up to 80 °C. Several experiments were conducted at 50 °C (Appendix A) but the method needs to be further optimized for these higher temperatures.

Further research on the effects of organic compounds on heterogeneous nucleation can be conducted using the methods used by Smetsers [4]. By using the improved MATLAB software, developed in parallel to this research (Appendix C), both rough and smooth surfaces can be analysed.

Bibliography

[1] Master Plan Geothermal Energy in the Netherlands. (May), 2018. 1

[2] Arjen Boersma, Frank Vercauteren, Hartmut Fischer, and Francesco Pizzocolo. Scaling Assessment, Inhibition and Monitoring of Geothermal Wells. *PROCEEDINGS, 43rd Workshop on Geothermal Reservoir Engineering Stanford University, Stanford, California, February 12-14, 2018*, 2018. 1, 4

[3] GFZ. Redefining geothermal fluid properties at extreme conditions to optimise future geothermal energy extraction - REFLECT, 2019. 1

[4] Tom Smetsers. Development of the scale-deposition flow rig. 2019. 1, 4, 5, 6, 7, 8, 13, 14, 23, 28, 29, 30, 38, 39

[5] Tung A. Hoang. *Mechanisms of Scale Formation and Inhibition*. Elsevier B.V., 2015. 3, 4, 5

[6] Olujide Sanni. Calcium carbonate surface / bulk scaling mechanisms and kinetics in a once-through in-situ flow visualization rig Olujide Samuel Sanni. 2016. 3, 7, 8, 14, 23

[7] J Moghadasi. Scale formation in Iranian oil reservoir and production equipment during water injection. *... on Oilfield Scale*, 2003. 4

[8] Loubna A Mohamed Gargoum. Calcium Carbonate Scale Formation under Multiphase Turbulent Conditions. 2018. 4, 5, 6, 8, 23

[9] J.W. Mullin. 5 - nucleation. In J.W. Mullin, editor, *Crystallization (Fourth Edition)*, pages 181 – 215. Butterworth-Heinemann, Oxford, fourth edition edition, 2001. 5

[10] Mike Crabtree, David Eslinger, Phil Fletcher, Matt Miller, Ashley Johnson, and George King. Fighting Scale Removal and Prevention. *Oilfield Review*, pages 30–45, 1999. 5

[11] M Ã Euvrard, F Membrey, C Filiatre, C Pignolet, and A Foissy. Kinetic study of the electrocrystallization of calcium carbonate on metallic substrates. 291:428–435, 2006. 5, 6

[12] J.W. Mullin. 6 - crystal growth. In J.W. Mullin, editor, *Crystallization (Fourth Edition)*, pages 216 – 288. Butterworth-Heinemann, Oxford, fourth edition edition, 2001. 6

[13] L Beaunier, C Gabrielli, G Poindessous, G Maurin, and R Rosset. Investigation of electrochemical calcareous scaling Nuclei counting and morphology. 501:41–53, 2001. 6

[14] J Chem Phys and Melvin Avrami. Kinetics of Phase Change . II Transformation-Time Relations for Random Distribution of Nuclei. 212(July 1939), 2004. 7

[15] K.S. Sorbie and N. Laing. How Scale Inhibitors Work: Mechanisms of Selected Barium Sulphate Scale inhibitors Across a Wide Temperature Range. pages 1–10, 2007. 7

[16] Abass A. Olajire. A review of oilfield scale management technology for oil and gas production. *Journal of Petroleum Science and Engineering*, 135:723–737, 2015. 7

[17] Oilfieldwiki. Scale inhibitor, 2016. 7

[18] R. C. Surdam, L. J. Crossey, E. S. Hagen, and H. P. Heasler. Organic-inorganic interactions and sandstone diagenesis. *American Association of Petroleum Geologists Bulletin*, 73(1):1–23, 1989. 9, 10

[19] Y. K. Kharaka and J. S. Hanor. Deep Fluids in Sedimentary Basins. *Treatise on Geochemistry: Second Edition*, 7:471–515, 2013. 9, 10

[20] Yaolin Liu and Baoxia Mi. Effects of organic macromolecular conditioning on gypsum scaling of forward osmosis membranes. *Journal of Membrane Science*, 450:153–161, 2014. 10

[21] I. Lebron and D. L. Suarez. Calcite nucleation and precipitation kinetics as affected by dissolved organic matter at 25C and pH $>$ 7.5. *Geochimica et Cosmochimica Acta*, 60(15):2765–2776, 1996. 10

[22] I. Lebrón and D. L. Suárez. Kinetics and mechanisms of precipitation of calcite as affected by PCO2 and organic ligands at 25C. *Geochimica et Cosmochimica Acta*, 62(3):405–416, 1998. 10

[23] Yasushi Kitano and Donald W. Hood. The influence of organic material on the polymorphic crystallization of calcium carbonate. *Geochimica et Cosmochimica Acta*, 29(1):29–41, 1965. 10

[24] Norio Wada, Kimihiro Yamashita, and Takao Umegaki. Effects of carboxylic acids on calcite formation in the presence of Mg2+ ions. *Journal of Colloid and Interface Science*, 212(2):357–364, 1999. 10, 23

[25] Norio Wada, Kiyoshi Kanamura, and Takao Umegaki. Effects of carboxylic acids on the crystallization of calcium carbonate. *Journal of Colloid and Interface Science*, 233(1):65–72, 2001. 10, 22

[26] Ian D. Block and Frank Scheffold. Modulated 3D cross-correlation light scattering: Improving turbid sample characterization. *Review of Scientific Instruments*, 81(12), 2010. 11

[27] N. Meulendijks, R. van Ee, R. Stevens, M. Mourad, M.A. Verheijen, N. Kambly, R. Armenta, and P. Buskens. Flow cell coupled dynamic light scattering for real-time monitoring of nanoparticle size during liquid phase bottom-up synthesis. *Applied Sciences*, 8(1):1–10, 1 2018. 11

[28] Malvern Panalytical. Derived count rate - what is it?, 2015. 12

[29] Marie Chaussemier, Ermane Pourmohtasham, Dominique Gelus, Nathalie Pécoul, Hubert Perrot, Jean Lédion, Hélène Cheap-Charpentier, and Olivier Horner. State of art of natural inhibitors of calcium carbonate scaling. A review article. *Desalination*, 356:47–55, 2015. 22

[30] John L. Wray and Farrington Daniels. Precipitation of Calcite and Aragonite. *Journal of the American Chemical Society*, 79(9):2031–2034, 1957. 23

[31] A. Declet, E. Reyes, and O. M. Suárez. Calcium carbonate precipitation: A review of the carbonate crystallization process and applications in bioinspired composites. *Reviews on Advanced Materials Science*, 44(1):87–107, 2016. 23

A. List of all experiments

	Name	SR	Acid	Acid Concentration (mmol/L)	Brine Solutions	Temp (°C)	pH	Flow (ml/m)
1	A-10	15	Acetic Acid	0,9	4	25	8,7	30
2	A-100	15	Acetic Acid	9	4	25	8,7	30
3	A-200	15	Acetic Acid	18	4	25	8,7	30
4	A-500	15	Acetic Acid	45	4	25	8,7	30
5	A-10-2	15	Acetic Acid	0,9	7	25	8,7	30
6	A-50	15	Acetic Acid	4,5	7	25	8,7	30
7	A-75	15	Acetic Acid	6,5	7	25	8,7	30
8	A-100-2	15	Acetic Acid	9	7	25	8,7	30
9	A-200-2	15	Acetic Acid	18	7	25	8,7	30
10	A-500-2	15	Acetic Acid	45	7	25	8,7	30
11	M-5	15	Malonic Acid	0,25	4	25	8,7	30
12	M-10,1	15	Malonic Acid	0,5	5	25	8,7	30
13	M-11,3	15	Malonic Acid	0,5	4	25	8,7	30
14	M-16,6	15	Malonic Acid	0,75	5	25	8,7	30
15	M-20,3	15	Malonic Acid	1	4	25	8,7	30
16	B-10	15	Benzoic Acid	0,4	4	25	8,7	30
17	B-10-2	15	Benzoic Acid	0,4	5	25	8,7	30
18	B-50	15	Benzoic Acid	2	4	25	8,7	30
19	B-100	15	Benzoic Acid	4	4	25	8,7	30
20	B-10-3	15	Benzoic Acid	0,4	10	25	8,7	30
21	C-1,8	15	Citric Acid	0,05	5	25	8,7	30
22	C-5,7	15	Citric Acid	0,1	5	25	8,7	30
23	C-2,1	15	Citric Acid	0,05	7	25	8,7	30
24	C-5,2	15	Citric Acid	0,1	7	25	8,7	30
25	C-10,1	15	Citric Acid	0,25	10	25	8,7	30
26	No additive	15	Na	na	4	25	8,7	30
27	50°C	15	Na	na	4	50	8,7	30
28	Static test	15	Na	na	7	25	8,7	0
29	5um filter	15	Na	na	7	25	8,7	30
30	10 um filter	15	Na	na	7	25	8,7	30
31	filtered solutions-1	15	Na	na	7	25	8,7	30
32	filtered solutions-2	15	Na	na	7	25	8,7	30
33	filtered solutions-3	15	Na	na	7	25	8,7	30
34	filtered solutions-4	15	Na	na	7	25	8,7	30
35	Plates	15	Na	na	7	25	8,7	30
36	Seed 0,4 ml	15	Na	na	7	25	8,7	30
37	No additive-2	15	na	na	10	25	8,7	30
38	A-11	50	Acetic Acid	0,9	1	25	8,7	30
39	A-50	50	Acetic Acid	4,5	1	25	8,7	30

40	A-100	**50**	Acetic Acid	9	1	25	8,7	30
41	A-200	**50**	Acetic Acid	18	1	25	8,7	30
42	A-500	**50**	Acetic Acid	45	1	25	8,7	30
43	A-1000	**50**	Acetic Acid	90	1	25	8,7	30
44	M-5	**50**	Malonic Acid	0,25	2	25	8,7	30
45	M-10	**50**	Malonic Acid	0,5	2	25	8,7	30
46	M-20	**50**	Malonic Acid	1	1	25	8,7	30
47	M-102	**50**	Malonic Acid	5	2	25	8,7	30
48	M-200	**50**	Malonic Acid	10	1	25	8,7	30
49	B-100	**50**	Benzoic Acid	4	2	25	8,7	30
50	B-201,1	**50**	Benzoic Acid	8	2	25	8,7	30
51	B-300	**50**	Benzoic Acid	12	2	25	8,7	30
52	B-400	**50**	Benzoic Acid	16	2	25	8,7	30
53	C-5	**50**	Citric Acid	0,1	3	25	8,7	30
54	C-10,2	**50**	Citric Acid	0,25	3	25	8,7	30
55	C-110	**50**	Citric Acid	25	3	25	8,7	30
56	C-10,5	**50**	Citric Acid	0,25	11	25	8,7	30
57	No Additive	**50**	Na	na	1	25	8,7	30
58	No Additive-2	**50**	na	na	11	25	8,7	30
59	50°C	**50**	na	na	1	50	8,7	30
60	Static test	**50**	Na	na	3	25	8,7	0
61	No additive	**5**	Na	na	6	25	8,7	30
62	No additive-2	**5**	Na	na	6	25	8,7	30
63	No additive-3	**5**	Na	na	6	25	8,7	30
64	Seed 0,6 ml pH 9,4	**5**	Na	na	6	25	9,4	30
65	Seed 0,6 ml pH 9,6 10um filter	**5**	Na	na	6	25	9,6	30
66	Seed 0,6 ml pH 9,6 5um filter	**5**	Na	na	6	25	9,6	30
67	No additive pH 9,5	**5**	Na	na	6	25	9,5	30
68	A-10	**9**	Acetic Acid	0,9	8	25	8,7	30
69	A-100	**9**	Acetic Acid	9	8	25	8,7	30
70	A-10-2	**9**	Acetic Acid	0,9	9	25	8,7	30
71	M-5	**9**	Malonic Acid	0,25	8	25	8,7	30
72	M-10	**9**	Malonic Acid	0,5	8	25	8,7	30
73	M-21,7	**9**	Malonic Acid	1	8	25	8,7	30
74	No additive	**9**	Na	na	8	25	8,7	30
75	10 um filter	**9**	Na	na	8	25	8,7	30

B. Exact concentrations

Table B.1: Exact Carboxylic acid concentrations

Saturation Ratio	**Acetic Acid** (mmol/L)	**Malonic Acid** (mmol/L)	**Benzoic Acid** (mmol/L)	**Citric Acid** (mmol/L)
9	0.873 8.734	0.274 0.505 1.043		
15	0.873 4.367 8.734 17.468 43.670	0.255 0.485 0.798 0.975	0.442 2.059 4.094	0,055 0,135 0.260
50	0,873 4.367 8.734 17.468 43.670 87.341	0.240 0.495 0.961 4.910 9.514	4,107 8.234 12.311 16.459	0.130 0.273 2.863

Table B.2: Exact concentrations of brine solutions

1 22-1-2020

	SR	Si	mass (g)	Actual mass (g)	Volume (L)	Nominal Concentration (M)	Actual Concentration (M)
SR50_CaCl2	50	1,699	6,909	6,9467	2	0,0235	0,02363
SR50_NaHCO3	50	1,699	3,948	3,9470	2	0,0235	0,02349

2 4-2-2020

	SR	Si	mass (g)	Actual mass (g)	Volume (L)	Nominal Concentration (M)	Actual Concentration (M)
SR50_CaCl2	50	1,699	6,909	6,8927	2	0,0235	0,02344
SR50_NaHCO3	50	1,699	3,948	3,9564	2	0,0235	0,02355

3 26-2-2020

	SR	Si	mass (g)	Actual mass (g)	Volume (L)	Nominal Concentration (M)	Actual Concentration (M)
SR50_CaCl2	50	1,699	6,909	6,8737	2	0,0235	0,02338
SR50_NaHCO3	50	1,699	3,948	3,9382	2	0,0235	0,02344

4 24-3-2020

	SR	Si	mass (g)	Actual mass (g)	Volume (L)	Nominal Concentration (M)	Actual Concentration (M)
SR15_CaCl2	15	1,176	2,940	2,9130	2	0,01	0,00991
SR15_NaHCO3	15	1,176	1,680	1,6860	2	0,01	0,01003

5 8-4-2020

	SR	Si	mass (g)	Actual mass (g)	Volume (L)	Nominal Concentration (M)	Actual Concentration (M)
SR15_CaCl2	15	1,176	2,940	2,918	2	0,01	0,00992
SR15_NaHCO3	15	1,176	1,680	1,7088	2	0,01	0,01017

6 28-4-2020

	SR	Si	mass (g)	Actual mass (g)	Volume (L)	Nominal Concentration (M)	Actual Concentration (M)
SR15_CaCl2	5	0,699	1,470	1,4566	2	0,005	0,00495
SR15_NaHCO3	5	0,699	0,840	0,8445	2	0,005	0,00503

7 22-4-2020

	SR	Si	mass (g)	Actual mass (g)	Volume (L)	Nominal Concentration (M)	Actual Concentration (M)
SR15_CaCl2	15	1,176	2,940	2,921	2	0,01	0,00993
SR15_NaHCO3	15	1,176	1,680	1,6792	2	0,01	0,00999

8 29-4-2020

	SR	Si	mass (g)	Actual mass (g)	Volume (L)	Nominal Concentration (M)	Actual Concentration (M)
SR15_CaCl2	9	0,954	1,103	1,1046	1	0,0075	0,00751
SR15_NaHCO3	9	0,954	0,630	0,6319	1	0,0075	0,00752

9 27-5-2020

	SR	Si	mass (g)	Actual mass (g)	Volume (L)	Nominal Concentration (M)	Actual Concentration (M)
SR15_CaCl2	9	0,954	1,103	1,0929	1	0,0075	0,00743
SR15_NaHCO3	9	0,954	0,630	0,6344	1	0,0075	0,00755

10 10-6-2020

	SR	Si	mass (g)	Actual mass (g)	Volume (L)	Nominal Concentration (M)	Actual Concentration (M)
SR15_CaCl2	15	1,176	2,940	2,9253	2	0,01	0,00995
SR15_NaHCO3	15	1,176	1,680	1,6786	2	0,01	0,00999

11 24-6-2020

	SR	Si	mass (g)	Actual mass (g)	Volume (L)	Nominal Concentration (M)	Actual Concentration (M)
SR15_CaCl2	50	1,699	3,455	3,4505	1	0,0235	0,02347
SR15_NaHCO3	50	1,699	1,974	1,9775	1	0,0235	0,02354

C. MATLAB GUI

As part of this study the MATLAB image Processing software developed by Smetsers [4] has been further optimized by creating a GUI and adding in new features. These additions will be discussed below.

C.1 GUI

The first step in the software developed by Smetsers [4] was to insert the variables needed to run the program, such as image size, measurement depth, etc. These variables needed to be inserted directly into the code which was not user friendly and prone to mistakes. A solution is the development of a GUI in which it is easy to set these variables and minimize mistakes while still retaining all the functionality and more. A screenshot of the GUI can be seen in figure C.2.

1. By clicking the "Load image list" button a popup will ask to select the first image in the directory with the images that need to be analyzed. All images with the same extension from this directory will be displayed in the listbox in the left corner of the app (8).
2. In this section of the app three variables can be set. The image height, image Width and the measurement depth are all used to calculate the particle characteristics of the detected particles.
3. In this section several variables can be set that are all used for the detection of the particles in the image. The optimal variables must be based on visual comparison of the processed images. When these variables are changed the changes will be shown in the bottom mid of the app (10).
    - Subdiff: This is the amount to subtract between morphological reconstruction in the imagerec function, the default is 10 and can be skipped if set to 0.
    - Threshold: This is the threshold level that distinguishes the foreground and background of the image.
    - Max intensity: This is the fraction of the maximum intensity that is required to be classified as a particle. All pixels that have an intensity below this value will be removed.
4. With the "Delete edge particles" switch the particles at the edge of the image can be removed and will not be analysed.
5. With the "Rough surface" switch the app can be switched between analysing smooth surfaces or rough surfaces. Analysing rough surfaces requires extra image processing which will be explained in chapter C.2.
6. In this section of the app a single image can be analysed and saved in the specified directory. This can be used to compare the results of different variables set in section (3) to reach the optimal variables.
7. In this section of the app multiple images can be analysed and will be automatically saved in the specified directory. No options can be changed in the app until the analyses is finished.
8. In this listbox all images in the selected directory will be shown. The selected file in this listbox will be shown in the app and processed (9)(10).
9. Here the original unprocessed image is shown that is selected in the listbox.
10. Here the processed image is shown that is selected in the listbox, in which the particles are shown in white.
11. Here the Particle area distribution is shown, with the particle count on the X-axis and the area on the Y-axis.
12. Here the diameter distribution and the mean diameter is shown, with the frequency on the X-axis and the diameter on the Y-axis.

C.2 Rough surface Background Correction

Originally, in this research it was planned to also look at heterogeneous nucleation. However this was picked up by a colleague intern. He encountered during image analysis of microscopic images of deposited scale, that the software developed by Smetsers [4] is unable to detect particles on rough surfaces. The old software can not distinguish the rough surface lines from the particles as can be seen in the right image in figure C.1. As part of my graduation project a solution to this problem has been developed and integrated into the code. By subtracting an image of the background from the image that needs to be analysed the rough surface stripes can be removed as can be seen in figure C.1. The background image must be taken before the start of the experiment. When analysing rough surface images the background image must be the first picture in the directory for the code to work. During the experiment care must be taken to minimize movement in the set up. Movement of the camera changes the background of the image thus stopping the code from correctly analysing the rough surface.

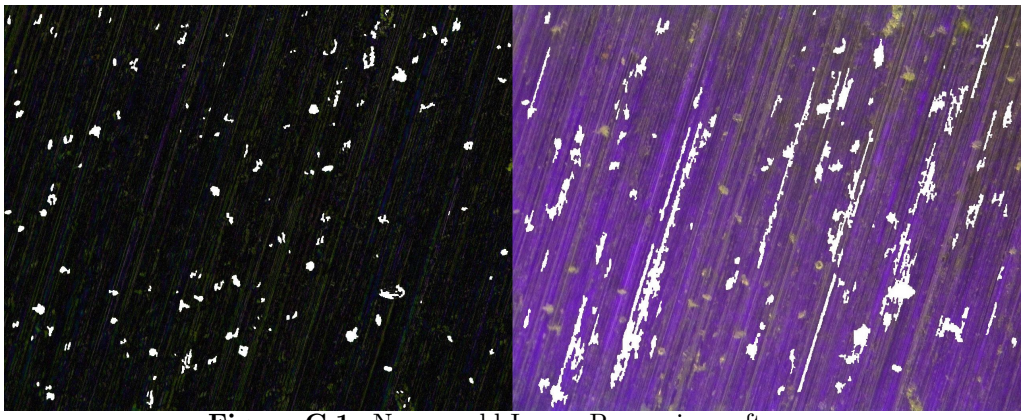

Figure C.1: New vs old Image Processing software

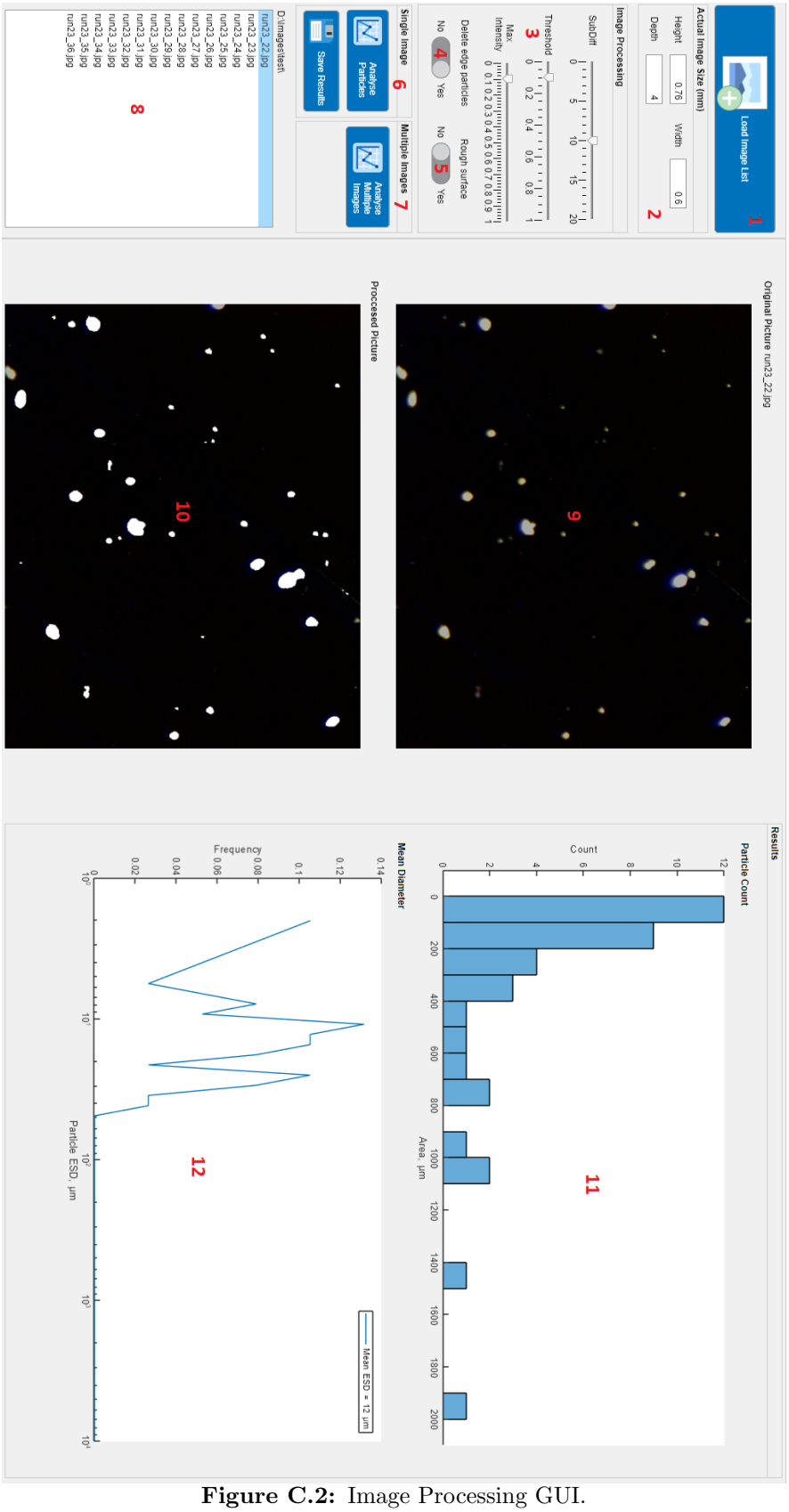

Figure C.2: Image Processing GUI.

D. Extra Experiments

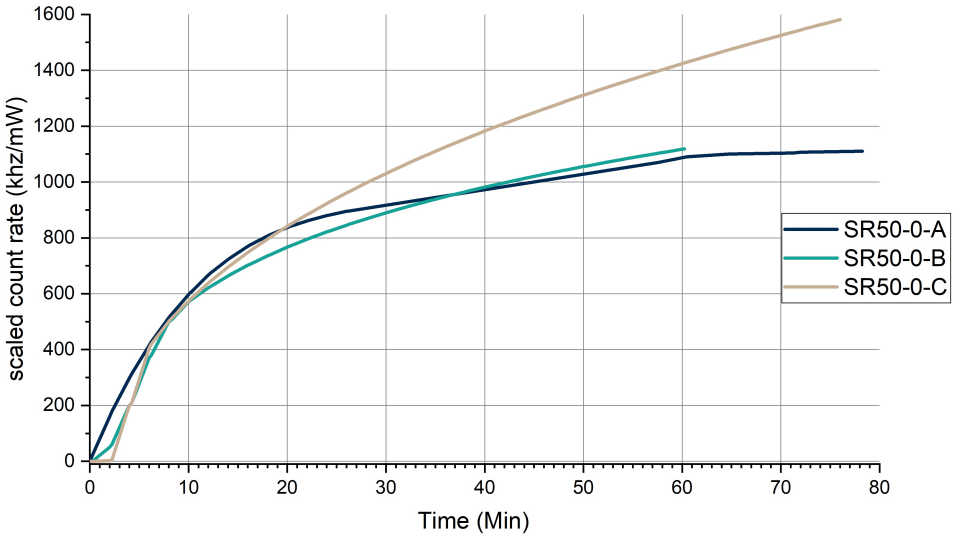

Figure D.1: Scaled count rate of $CaCO_3$ precipitation at SR50, three identical experiments were conducted with no addition of any acid.

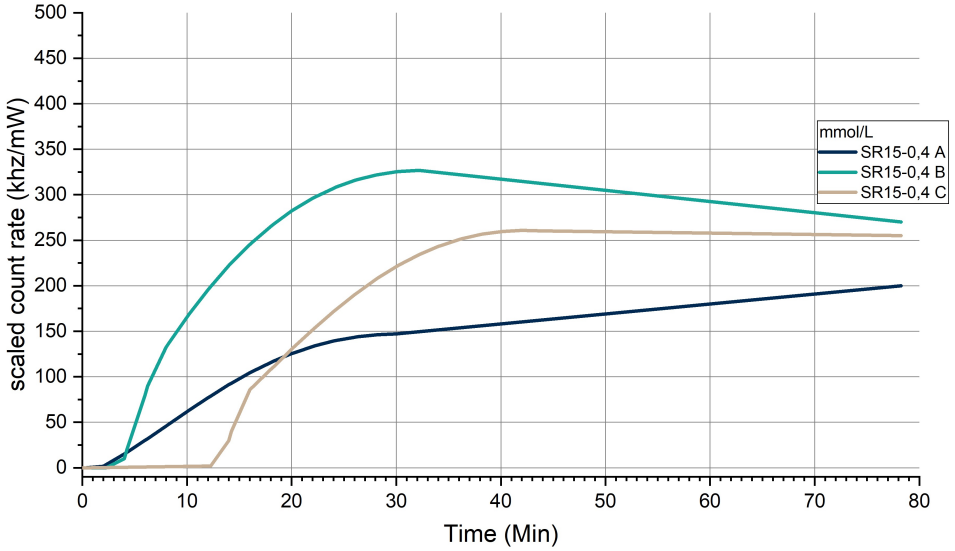

Figure D.2: Scaled count rate of $CaCO_3$ precipitation at SR15 after addition of 0,4 mmol/L Benzoic acid

E. Homogenous vs heterogenous Images

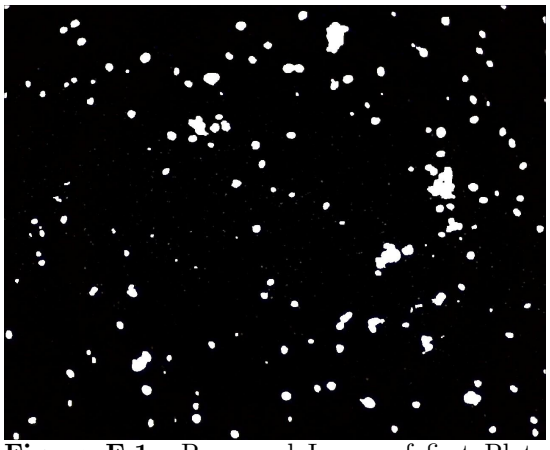

Figure E.1: Processed Image of first Plate T=20 (749x)

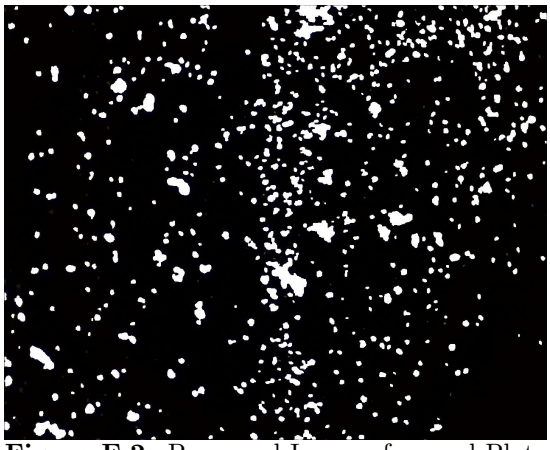

Figure E.2: Processed Image of second Plate T=25 (749x)

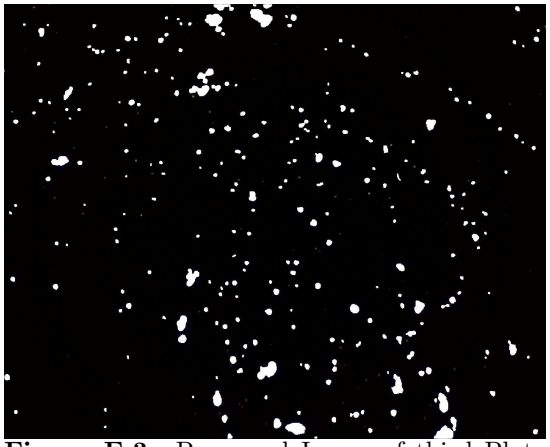

Figure E.3: Processed Image of third Plate T=30 (749x)

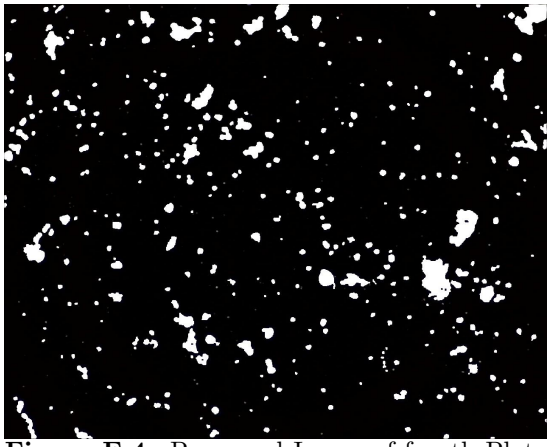

Figure E.4: Processed Image of fourth Plate T=35 (749x)

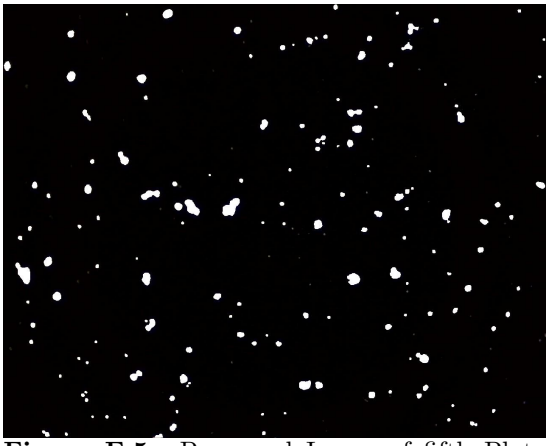

Figure E.5: Processed Image of fifth Plate T=40 (749x)

F. List of SEM Samples

SR	Sample # *	Name	Additive:	Observed morphologies			
				cubes	flowers	spheres	needles
sr5	67	No additive pH 9,5	no additive	x			
	64	Seed 0,6 ml pH 9,4		x		x	
sr9	74	No additive	no additive	x			x
	68	A-10	acetic acid	x	x		x
	71	M-5	malonic	x	x		
sr15	35	Seed 0,4 ml	no additive	x	x	x	
	25	No additive		x	x	x	
	26	50 C		x			x
	15	A-10	acetic	x	x	x	
	2	A-100		x	x	x	
	3	A-200		x	x	x	
	4	A-500		x	x	x	
	11	M-5	malonic	x	x	x	
	15	M-20,3		x		x	
	17	B-10	benzoic	x	x	x	
	18	B-50		x		x	
	20	C-1,8	citric	x		x	
	21	C5,7					
sr50	57	no additive	no additive	x	x	x	
	59	50 C		x	x		x
	40	A-100	accetic acid	x	x	x	
	42	A-500		x	x	x	x
	45	M-10	malonic acid	x	x	x	
	47	M-100		x	x	x	x
	54	C-10	Citric acid	x		x	
	55	C-110					

* For list of samples see appendix A.